The alarmin interleukin-33 promotes the expansion and preserves the stemness of Tcf-1+ CD8+ T cells in chronic viral infection

Marx, Anna-Friederike; Kallert, Sandra M; Brunner, Tobias M; Villegas, José A; Geier, Florian; Fixemer, Jonas; Abreu-Mota, Tiago; Reuther, Peter; Bonilla, Weldy V; Fadejeva, Jelizaveta; Kreutzfeldt, Mario; Wagner, Ingrid; Aparicio-Domingo, Patricia; Scarpellino, Leo [**and 13 more**]

Article

Immunity

The alarmin interleukin-33 promotes the expansion and preserves the stemness of Tcf-1^{+} CD8^{+} T cells in chronic viral infection

Graphical abstract

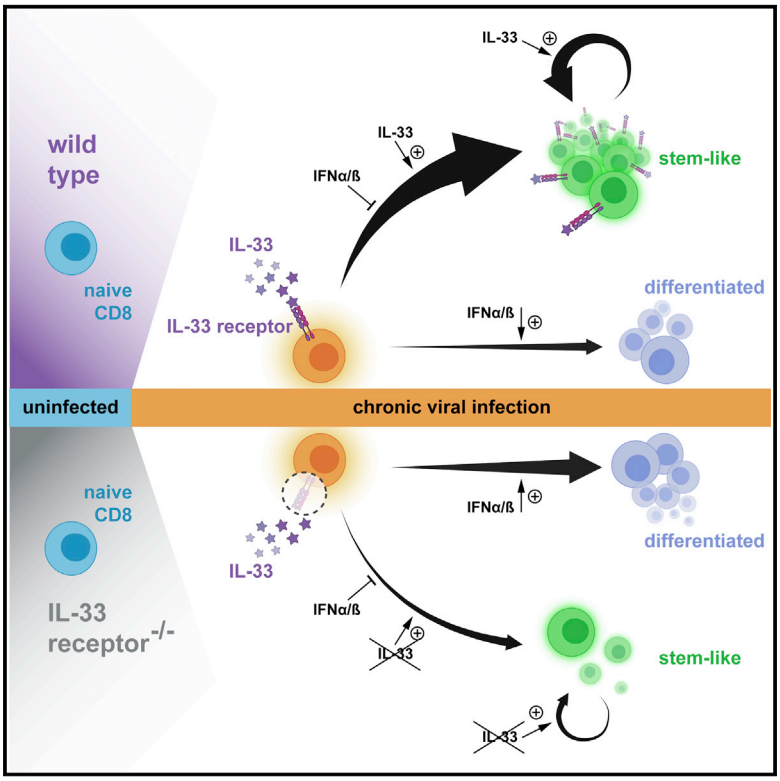

Highlights

- Interleukin-33 (IL-33) promotes the expansion of stem-like CD8 T cells (CD8^{+}SL)
- IL-33 signals augment chromatin accessibility of CD8^{+}SL in chronic viral infection
- IL-33 prevents the loss of Tcf-1 expression by balancing type I interferon effects
- IL-33 signaling to CD8^{+}SL preserves these cells' stemness and re-expansion capacity

Authors

Anna-Friederike Marx, Sandra M. Kallert, Tobias M. Brunner, ..., Sanjiv A. Luther, Max Löhning, Daniel D. Pinschewer

Correspondence

a.marx@unibas.ch (A.-F.M.), max.loehning@charite.de (M.L.), daniel.pinschewer@unibas.ch (D.D.P.)

In brief

Stem-like Tcf-1-expressing CD8 T cells (CD8^{+}SL) are key to immune defense in chronic infection and cancer, but the cytokine signals that promote CD8^{+}SL cell expansion and stemness remain undefined. Marx et al. reveal that interleukin-33 assumes this role by balancing type I interferon signals and augmenting chromatin accessibility of CD8^{+}SL.

Marx et al., 2023, Immunity *56*, 1–16
April 11, 2023
https://doi.org/10.1016/j.immuni.2023.01.029

CellPress

Immunity

CellPress
OPEN ACCESS

Article

The alarmin interleukin-33 promotes the expansion and preserves the stemness of Tcf-1$^+$ CD8$^+$ T cells in chronic viral infection

Anna-Friederike Marx,[1,13,*] Sandra M. Kallert,[1,13] Tobias M. Brunner,[2,3,13] José A. Villegas,[4] Florian Geier,[5,6] Jonas Fixemer,[1] Tiago Abreu-Mota,[1] Peter Reuther,[1] Weldy V. Bonilla,[1] Jelizaveta Fadejeva,[2,3] Mario Kreutzfeldt,[7,12] Ingrid Wagner,[7,12] Patricia Aparicio-Domingo,[4] Leo Scarpellino,[4] Mélanie Charmoy,[8] Daniel T. Utzschneider,[9] Claudia Hagedorn,[10] Min Lu,[1] Karen Cornille,[1] Karsten Stauffer,[1] Florian Kreppel,[10] Doron Merkler,[7,12] Dietmar Zehn,[11] Werner Held,[8] Sanjiv A. Luther,[4] Max Löhning,[2,3,*] and Daniel D. Pinschewer[1,14,*]

[1]Department of Biomedicine, Division of Experimental Virology, University of Basel, 4055 Basel, Switzerland
[2]Experimental Immunology and Osteoarthritis Research, Department of Rheumatology and Clinical Immunology, Charité – Universitätsmedizin Berlin, corporate member of Freie Universität Berlin and Humboldt-Universität zu Berlin, 10117 Berlin, Germany
[3]Pitzer Laboratory of Osteoarthritis Research, German Rheumatism Research Center (DRFZ), a Leibniz Institute, 10117 Berlin, Germany
[4]Department of Immunobiology, University of Lausanne, 1066 Epalinges, Switzerland
[5]Department of Biomedicine, Bioinformatics Core Facility, University Hospital Basel, 4031 Basel, Switzerland
[6]Swiss Institute of Bioinformatics, Basel, Switzerland
[7]Department of Pathology and Immunology University of Geneva, Geneva, Switzerland
[8]Department of Oncology, University of Lausanne, 1066 Epalinges, Switzerland
[9]Department of Microbiology and Immunology, Peter Doherty Institute for Infection and Immunity, University of Melbourne, Melbourne, VIC 3000, Australia
[10]Witten/Herdecke University (UW/H), Faculty of Health/School of Medicine, Stockumer Str. 10, 58453 Witten, Germany
[11]Division of Animal Physiology and Immunology, School of Life Sciences Weihenstephan, Technical University of Munich, 85354 Freising, Germany
[12]Division of Clinical Pathology, Geneva University Hospital, 1211 Geneva, Switzerland
[13]These authors contributed equally
[14]Lead contact
*Correspondence: a.marx@unibas.ch (A.-F.M.), max.loehning@charite.de (M.L.), daniel.pinschewer@unibas.ch (D.D.P.)
https://doi.org/10.1016/j.immuni.2023.01.029

SUMMARY

T cell factor 1 (Tcf-1) expressing CD8$^+$ T cells exhibit stem-like self-renewing capacity, rendering them key for immune defense against chronic viral infection and cancer. Yet, the signals that promote the formation and maintenance of these stem-like CD8$^+$ T cells (CD8$^+$SL) remain poorly defined.

Studying CD8$^+$ T cell differentiation in mice with chronic viral infection, we identified the alarmin interleukin-33 (IL-33) as pivotal for the expansion and stem-like functioning of CD8$^+$SL as well as for virus control. IL-33 receptor (ST2)-deficient CD8$^+$ T cells exhibited biased end differentiation and premature loss of Tcf-1. ST2-deficient CD8$^+$SL responses were restored by blockade of type I interferon signaling, suggesting that IL-33 balances IFN-I effects to control CD8$^+$SL formation in chronic infection. IL-33 signals broadly augmented chromatin accessibility in CD8$^+$SL and determined these cells' re-expansion potential.

Our study identifies the IL-33-ST2 axis as an important CD8$^+$SL-promoting pathway in the context of chronic viral infection.

INTRODUCTION

CD8$^+$ T cells have long been established as a cornerstone of immune control in persistent viral infection and cancer.[1–11] More recently, evidence has accumulated that the CD8$^+$ T cell response in both types of chronic disease is maintained by a distinct subset of memory-like or stem-like CD8$^+$ T cells (CD8$^+$SL).[12–20] CD8$^+$SL exhibit robust expansion potential as well as self-renewing and differentiation capacity in both mice and humans. They depend on and are identified by their expression of the transcription factor T cell factor-1 (Tcf-1) (encoded by the *Tcf7* gene)[12,13,16] and express Ly108 (encoded by the *Slamf6* gene)[21] as well as CXCR5[13,14] in combination with inhibitory receptors such as programmed cell death protein 1 (PD-1). In addition to its prominent expression in the context of chronic infection Tcf-1 is also expressed by all naive T cells as well as by a majority of memory T cells emerging from resolved acute infection.[22,23] Importantly, Tcf-1$^+$ CD8$^+$SL not only ascertain

Please cite this article in press as: Marx et al., The alarmin interleukin-33 promotes the expansion and preserves the stemness of Tcf-1+ CD8+ T cells in chronic viral infection, Immunity (2023), https://doi.org/10.1016/j.immuni.2023.01.029

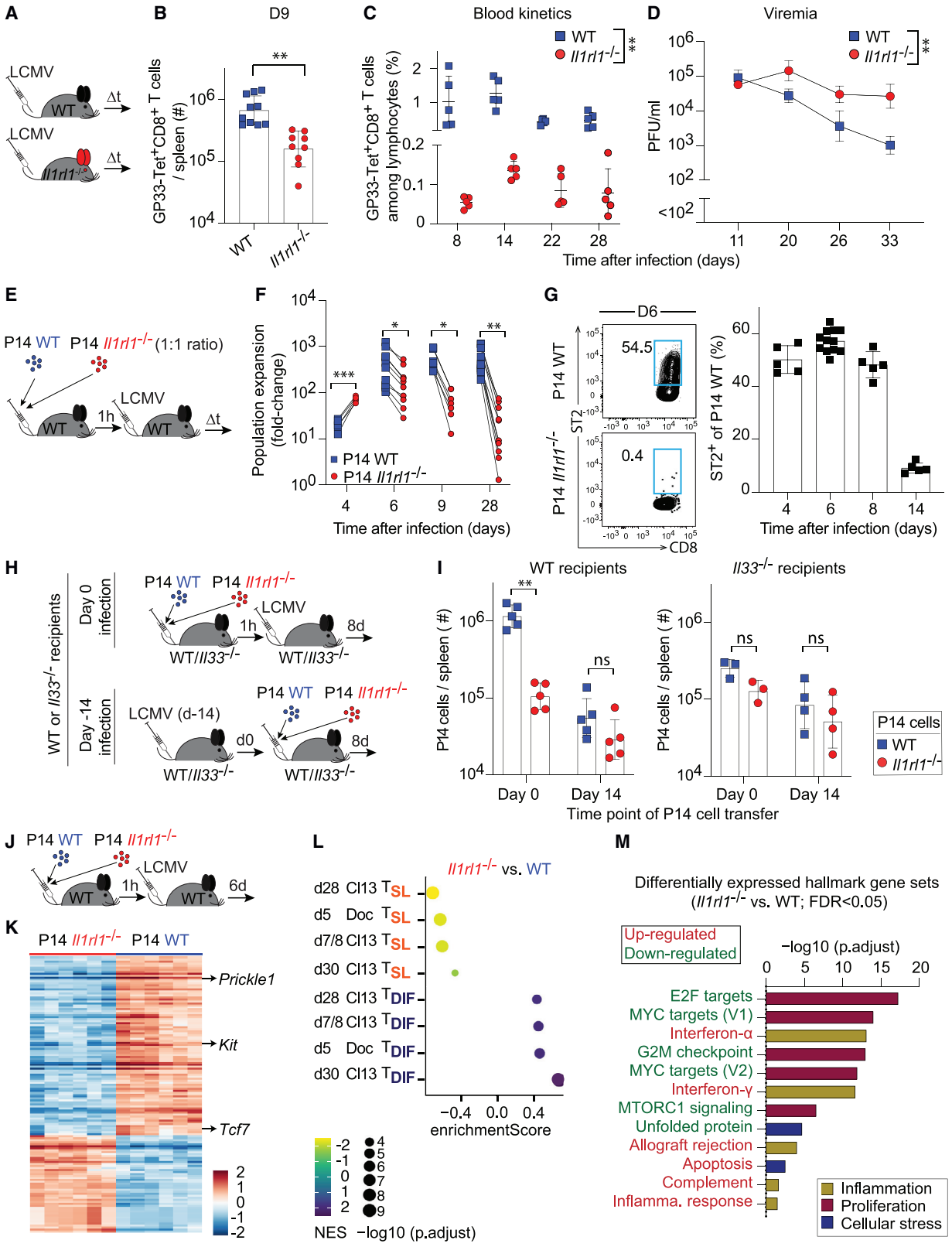

Figure 1. Impact of ST2 signaling on the expansion and differentiation of CD8+ T cells in chronic viral infection

(A–D) WT and *Il1rl1*$^{-/-}$ mice were infected with LCMV Cl13. GP33-Tet+ CD8+ T cells were enumerated in spleen (B) and in blood (C). Gating strategy is shown in Figure S1A. Viremia was determined (D).

(legend continued on next page)

Please cite this article in press as: Marx et al., The alarmin interleukin-33 promotes the expansion and preserves the stemness of Tcf-1$^+$ CD8$^+$ T cells in chronic viral infection, Immunity (2023), https://doi.org/10.1016/j.immuni.2023.01.029

long-term T cell population maintenance under conditions of chronic antigen exposure,[12,13,15] but they also represent the cellular source for differentiated cells that lack Tcf-1 but retain PD-1 and express granzyme B and have cytolytic potential. This process is augmented by the blockade of the inhibitory PD-1 pathway and depends on the presence of CD8$^+$SL,[12,13] highlighting the wide-ranging translational implications of the CD8$^+$SL subset. Transcriptional[12,13] and epigenetic programs[24,25] suggest that the bifurcation of CD8$^+$SL from effector cells starts in the first few days after activation,[23,26] and their transcriptional regulation has been studied in detail.[16,27,28] Moreover, type I interferons (IFN-I) promote CD8$^+$ T cell effector differentiation at the expense of the Tcf-1$^+$ CD8$^+$SL pool, such that IFN-I receptor (IFNAR) blockade in chronic viral infection augments the CD8$^+$SL population in an IL-27-dependent manner.[16,29] The differentiation-promoting effects of IFN-I on CD8$^+$ T cell responses comprise direct as well as indirect effects.[30–35] Importantly, however, signals that warrant the formation of Tcf-1$^+$ CD8$^+$SL in the presence of detrimental IFN-I effects remain largely undefined.

Over the course of the past decade the alarmin interleukin-33 (IL-33), an IL-1 family member,[36] has emerged as a key driver of protective CD8$^+$ T cell responses to several RNA and DNA viruses.[37–40] Upon infection, IL-33 is released from T zone fibroblastic reticular cells (FRCs) of the spleen and lymph nodes.[41,42] It signals through its receptor ST2 (encoded by the *Il1rl1* gene) also referred to as T1 or IL1RL1,[36,43,44] which is expressed on activated CD8$^+$ T cells and furthers the clonal expansion and effector differentiation of CD8$^+$ T cells in the context of acute viral infection.[37,42,45] Replicating viral vector platforms can trigger the IL-33-ST2 axis to improve the efficacy of therapeutic tumor vaccination.[41,46] The pathway can also be exploited by co-delivering IL-33 in DNA vaccines or as recombinant protein.[47–50] In contrast, the contribution of ST2 signaling to CD8$^+$ T cell-dependent immune defense in chronic viral infection remains less well defined.[37,42] Impaired control of chronic but not acute lymphocytic choriomeningitis virus (LCMV) infection has been observed in ST2- and IL-33-deficient mice[37,42]; however, the impact of IL-33 signals on CD8$^+$ T cell differentiation in the chronic infection context remains to be investigated.

Here, we show that IL-33 signaling maintains the population size and preserves the stemness of Tcf-1$^+$ CD8$^+$SL. IL-33 signaling through ST2 on antiviral CD8$^+$ T cells profoundly enhanced these cells' re-expansion capacity, which was associated with broadly augmented chromatin accessibility. Moreover, it counterbalanced IFN-I effects to maintain CD8$^+$SL stemness in the context of chronic viral infection.

RESULTS

ST2 signaling impacts the expansion and differentiation of CD8$^+$ T cells in chronic viral infection

To investigate the importance of IL-33-ST2 signaling for CD8$^+$ T cell responses to chronic viral infection, we inoculated *Il1rl1*$^{-/-}$ and wild-type (WT) control mice with LCMV clone 13 (Figure 1A). 9 days later, spleens of *Il1rl1*$^{-/-}$ mice harbored approximately 5 times less CD8$^+$ T cells reactive to the immunodominant viral GP33 epitope than WT control animals (Figure 1B), and analogous differences were observed in peripheral blood throughout day 28 of the experiment (Figure 1C). These differences translated into impaired virus control in *Il1rl1*$^{-/-}$ mice, as expected[37,42] (Figure 1D). To selectively assess the CD8$^+$ T cell-intrinsic role of ST2 signaling we studied mixed WT: *Il1rl1*$^{-/-}$ bone marrow chimeric mice (Figures S1B–S1D). Consistent with earlier findings in acute LCMV infection[37,45] WT CD8$^+$ T cells expanded to >10-fold higher numbers than competing *Il1rl1*$^{-/-}$ CD8$^+$ T cells in the same host. To corroborate and further investigate this CD8$^+$ T cell-intrinsic role of ST2 signaling in the chronic infection context, we co-transferred equal numbers of LCMV GP33-specific T cell receptor (TCR)-transgenic CD8$^+$ T cells (P14 cells),[51] either ST2-deficient or -sufficient (P14 *Il1rl1*$^{-/-}$;P14 WT) into WT recipients that were challenged with LCMV (Figure 1E). The expansion of P14 WT cells was superior to P14 *Il1rl1*$^{-/-}$ cells on days 6, 9, and 28 (Figure 1F), matching the above observations on defective CD8$^+$ T cell responses in *Il1rl1*$^{-/-}$ animals and corroborating the CD8$^+$ T cell-intrinsic role of ST2 signaling in chronic viral infection. However, P14 *Il1rl1*$^{-/-}$ cells outnumbered P14 WT cells on day 4 after infection (Figure 1F), suggesting that the cells' initial proliferative capacity was unimpaired but was not sustained in the long run.

ST2 is not expressed in naive CD8$^+$ cells but more than half of the P14 WT cells expressed ST2 (ST2$^+$) on days 4, 6, and 8 and the proportion of ST2$^+$ cells declined thereafter, reaching ~10% by day 14 (Figure 1G). IL-33 release from FRCs is largely confined to the first few days after LCMV infection.[42] Accordingly, P14 *Il1rl1*$^{-/-}$ cells expanded comparably to P14 WT cells when transferred on day 14 after infection (Figures 1H and 1I)

(E–G) Equal numbers of P14 WT (CD45.1/2) and P14 *Il1rl1*$^{-/-}$ (CD45.1/1) cells were transferred into WT (CD45.2) recipients followed by LCMV infection. Population expansion (fold change to input) in spleen (F). Gating strategy is shown in Figure S1E. Representative FACS plots and quantification of ST2 expression on day 6 (G). The percentage of gated populations is indicated. The bar graph reports the percentage of ST2-expressing P14 WT cells.
(H and I) We co-transferred P14 WT and P14 *Il1rl1*$^{-/-}$ cells on day 0 into WT and *Il33*$^{-/-}$ mice that were either infected with LCMV the same day (day 0) or 14 days earlier (day 14). P14 cells were enumerated 8 days after transfer.
(J–M) We co-transferred P14 WT and P14 *Il1rl1*$^{-/-}$ cells into WT mice, followed by LCMV infection and P14 cell sorting (Figure S1E) for RNA-seq on day 6. (K) Heatmap of hierarchically clustered differentially expressed genes; absolute $\log_2$ fold change, $\log_2$FC > 1.5; false discovery rate (FDR) adjusted p value < 0.05 (Table S1). Each column represents one mouse. (L) The gene set in (K) was subject to an enrichment test for end-differentiated (DIF) versus stem-like (SL) CD8$^+$ T cell signatures (Table S2). The bubble size reports the adjusted p value. NES, normalized enrichment score. (M) Differentially expressed hallmark gene sets from MSigDB (FDR < 0.05; FDR adjusted p value < 0.05).
Data from one representative out of two similar experiments are shown in (C), (D), (I), and (G) for days 4, 8, and 14, combined data from two independent experiments are reported in (B), (F), and (G) for day 6. Symbols in (B), (C), (F), (G), and (I) show individual mice (bars represent means ± SD), in (D) the mean ± SD of five mice. Unpaired two-tailed Student's t test was performed in (B), time-course analysis using a mixed model two-way ANOVA (C and D), two-way ANOVA with Sidak's post-test in (F), two-way ANOVA with Tukey's multiple comparison test in (I). *p < 0.05; **p < 0.01. ns: not statistically significant.
Please also see Figure S1.

Please cite this article in press as: Marx et al., The alarmin interleukin-33 promotes the expansion and preserves the stemness of Tcf-1+ CD8+ T cells in chronic viral infection, Immunity (2023), https://doi.org/10.1016/j.immuni.2023.01.029

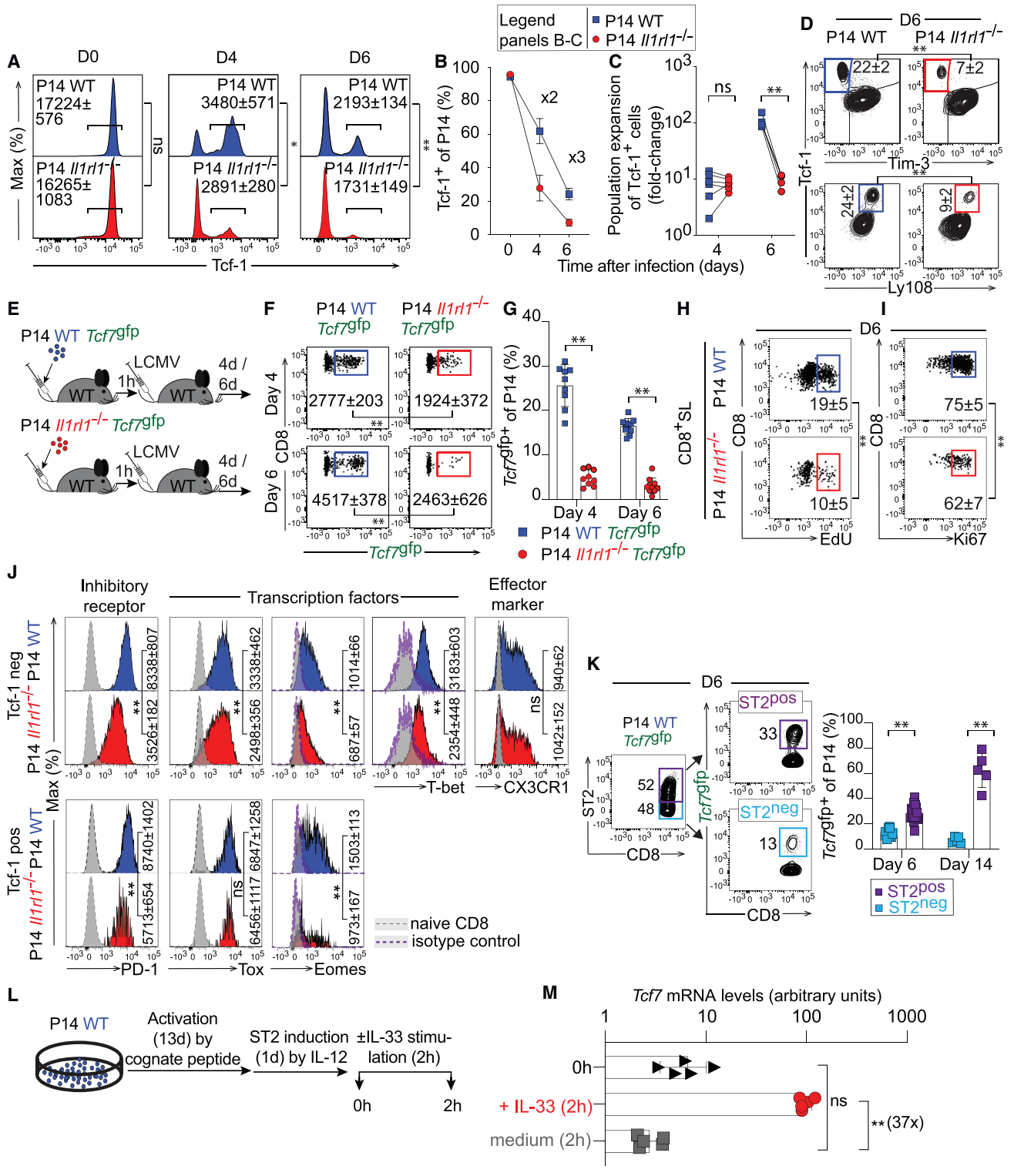

Figure 2. IL-33 signaling promotes Tcf-1 expression by CD8+ T cells

(A–D) In a setup as outlined in Figure 1E, we determined Tcf-1 expression by P14 WT and P14 *Il1rl1*$^{-/-}$ cells on days 0, 4, and 6 after LCMV infection. (A) MFI of Tcf-1+ cells reported as mean ± SD. The percentage of gated cells is reported in (B), the population expansion in (C). Representative FACS plots (day 6) are shown in (D). Numbers in (A) and (D) indicate the mean ± SD.

(E–G) We transferred P14 WT *Tcf7*^{gfp} and P14 *Il1rl1*$^{-/-}$ *Tcf7*^{gfp} cells into WT mice followed by LCMV infection. Representative FACS plots in (F) show *Tcf7*^{gfp} reporting on days 4 and 6 (MFI reported as mean ± SD) and the frequency of gated cells is indicated (G).

(legend continued on next page)

Please cite this article in press as: Marx et al., The alarmin interleukin-33 promotes the expansion and preserves the stemness of Tcf-1$^+$ CD8$^+$ T cells in chronic viral infection, Immunity (2023), https://doi.org/10.1016/j.immuni.2023.01.029

but exhibited the aforementioned expansion deficit when transferred prior to infection. As expected, these differences were largely abrogated when P14 *Il1rl1*$^{-/-}$ and P14 WT cells were challenged in *Il33*$^{-/-}$ hosts, altogether suggesting the bioavailability of IL-33 and its impact on antiviral CD8$^+$ T cell responses are largely confined to an early time window after infection.

To assess the effect of ST2 signaling on gene expression profiles of CD8$^+$ T cell in chronic viral infection we sorted P14 WT and P14 *Il1rl1*$^{-/-}$ cells on day 6 after LCMV infection for RNA sequencing (RNA-seq) analysis (Figure 1J). Among the 90 genes that were downregulated in P14 *Il1rl1*$^{-/-}$ cells we found hallmark genes of CD8$^+$SL such as *Tcf-7* (encoding Tcf-1), *Prickle1*, and *Kit*[13] (Figure 1K; Table S1). A comparison to published datasets[12,21,26,52,53] confirmed that *Il1rl1*$^{-/-}$ P14 cells exhibited an impaired expression of CD8$^+$SL signature genes with a concomitant enrichment in gene sets related to end-differentiation (Figure 1L; Table S2). Equally likely, the sorted P14 *Il1rl1*$^{-/-}$ cells may have comprised a reduced proportion of Tcf-1$^+$ CD8$^+$SL cells, emerging in this bulk analysis as a downregulation of CD8$^+$SL signature genes. Gene set enrichment analyses revealed further that, among other pathways, *Il1rl1*$^{-/-}$-deficient CD8$^+$ T cells displayed accentuated inflammation-related signatures including an exaggerated interferon-α response (Figures 1M and S1F). Given that the P14 WT and P14 *Il1rl1*$^{-/-}$ cells were co-transferred, responding to LCMV in the same recipient, and thus were exposed to the same inflammatory context and viral load (Figure 1J), these data implied that ST2 signaling attenuated IFN-I gene signatures at the level of individual CD8$^+$ T cells. In summary, our findings suggested that ST2-deficient CD8$^+$ T cells responded to chronic viral challenge with an initially overshooting but subsequently impaired proliferative response (Figure 1F), which was associated with reduced expression of stemness-related genes and with an exaggerated IFN-I-induced transcriptional response (Figures 1K–1M).

IL-33 signaling promotes Tcf-1 expression by CD8$^+$ T cells

In light of the above findings that *Il1rl1*$^{-/-}$ mice had an impaired expression of CD8$^+$SL signature genes (Figures 1K and 1L), we assessed expression of the transcription factor Tcf-1 in P14 WT and P14 *Il1rl1*$^{-/-}$ cells. As expected,[54] both types of cells uniformly expressed Tcf-1 protein in their naive state but a 2- to 3-fold lower proportion of P14 *Il1rl1*$^{-/-}$ cells retained Tcf-1 on days 4 and 6 after infection, and Tcf-1 expression levels (geometric mean fluorescence intensity, MFI) within the residual population of Tcf-1$^+$ P14 *Il1rl1*$^{-/-}$ cells were reduced (Figures 2A and 2B). As a consequence of the overshooting overall expansion of P14 *Il1rl1*$^{-/-}$ cells on day 4 of the response (compare Figure 1F), the population expansion of Tcf-1$^+$ P14 *Il1rl1*$^{-/-}$ cells was comparable to Tcf-1$^+$ P14 WT cells at this time point (Figure 2C). Between day 4 and day 6, however, Tcf-1$^+$ P14 *Il1rl1*$^{-/-}$ cells failed to expand further, whereas WT Tcf-1$^+$ P14 cells expanded ~10-fold (Figure 2C). This relative deficiency in CD8$^+$SL expansion and/or survival of P14 *Il1rl1*$^{-/-}$ cells was also evident in a reduced proportion of Ly108$^+$ Tcf-1$^+$ and Tcf-1$^+$ Tim-3$^-$ cells (Figure 2D), and it affected the CD69-positive and CD69-negative subsets of Ly108$^+$ P14 cells[25] to a comparable extent (Figures S2A–S2C). We extended these studies to P14 WT and P14 *Il1rl1*$^{-/-}$ cells carrying a green fluorescent *Tcf7* reporter allele (*Tcf7*^{gfp}).[12] In concert with the above protein staining data, the proportion of *Tcf7*$^{gfp+}$ cells and the extent of *Tcf7*^{gfp} reporting by P14 *Il1rl1*$^{-/-}$ cells were substantially lower than in P14 WT *Tcf7*^{gfp} cells, both on days 4 and 6 (Figures 2E–2G). ST2 expression by CD8$^+$ T cells was thus essential for the expansion of Tcf-1$^+$ CD8$^+$SL.

In a complementary experimental approach, we found fewer Tcf-1 reporting P14 WT *Tcf7*^{gfp} cells when LCMV challenge was performed in *Il33*$^{-/-}$ recipients instead of WT hosts, and the extent of *Tcf7*^{gfp} reporting was also reduced (Figures S2D–S2G). Moreover, the CD8$^+$SL compartment of P14 *Il1rl1*$^{-/-}$ cells exhibited somewhat reduced proliferative activity as determined by EdU incorporation and a lower proportion of Ki67^{hi} cells (Figures 2H and 2I) altogether indicating that IL-33 was needed to maintain and/or expand the Tcf-1$^+$ CD8$^+$SL population between day 4 and day 6. An extended phenotypic comparison of P14 WT and P14 *Il1rl1*$^{-/-}$ cells on day 6 of chronic LCMV infection revealed that *Il1rl1*-deficiency reduced the expression levels of the stemness-promoting transcription factor Eomes[55] and of the inhibitory receptor PD-1, which is expressed by CD8$^+$SL.[12,21] These differences were observed in both, Tcf-1$^+$ and Tcf-1$^-$ P14 cells, whereas the transcription factor Tox was reduced in the Tcf-1$^-$ but not Tcf-1$^+$ subset of P14 *Il1rl1*$^{-/-}$ cells (Figure 2J). The effector cell-associated transcription factor T-bet as well as the CD8$^+$ effector/homing marker CX3CR1[56,57] were analyzed in the Tcf-1$^-$ subset. T-bet expression levels were reduced in ST2-deficient cells, whereas CX3CR1 staining intensity was unaffected (Figure 2J). However, the Tcf-1$^+$ CX3CR1$^-$ and the Tcf-1$^-$ CX3CR1$^+$ subsets of P14 *Il1rl1*$^{-/-}$ cells were reduced in number, whereas the abundance of Tcf-1$^-$CX3CR1$^-$ cells was not significantly affected by ST2

(H and I) In an experiment as in (A) 5 h EdU incorporation and Ki67 expression were determined on day 6. Representative FACS plots are gated on CD8$^+$ Ly108$^+$ Tim-3$^-$ cells (CD8$^+$SL), mean ± SD is shown.

(J) In an experiment as in (A) expression levels of transcription factors and surface markers were determined on day 6 after gating on Tcf-1$^+$ or Tcf-1$^-$ cells (MFI reported as mean ± SD).

(K) P14 WT *Tcf7*^{gfp} cells were transferred into WT recipients followed by LCMV infection as outlined in (E) and stained for ST2. ST2-positive and -negative cells were analyzed for *Tcf7*^{gfp} reporting on days 6 and 14. Representative FACS plots from day 6 are shown, the frequency of gated cells is indicated. P14 *Il1rl1*$^{-/-}$ *Tcf7*^{gfp} CD8$^+$ T cells served as staining control.

(L and M) We activated P14 WT cells *in vitro* using their cognate GP33 peptide and induced ST2 receptor expression by exogenous IL-12, followed by stimulation with recombinant IL-33 or mock for 2 h. *Tcf7* mRNA levels were determined (arbitrary units relative to *Hprt*; M).

Representative data from two independent experiments are shown in (A)–(D), (F), (H)–(J), (M), and (K) for day 14. (G and K for day 6) report data from two combined experiments. Symbols in (A, B, five mice per group), and bars represent means ± SD. Symbols in (C), (G), and (K) represent individual mice or individual cultures (M). Paired two-tailed Student's t test was used in (A), (C), (D), and (F)–(K), one-way ANOVA with Dunnett's post-test (M). *$p < 0.05$; **$p < 0.01$, ns: not statistically significant.

Please also see Figure S2.

Please cite this article in press as: Marx et al., The alarmin interleukin-33 promotes the expansion and preserves the stemness of Tcf-1+ CD8+ T cells in chronic viral infection, Immunity (2023), https://doi.org/10.1016/j.immuni.2023.01.029

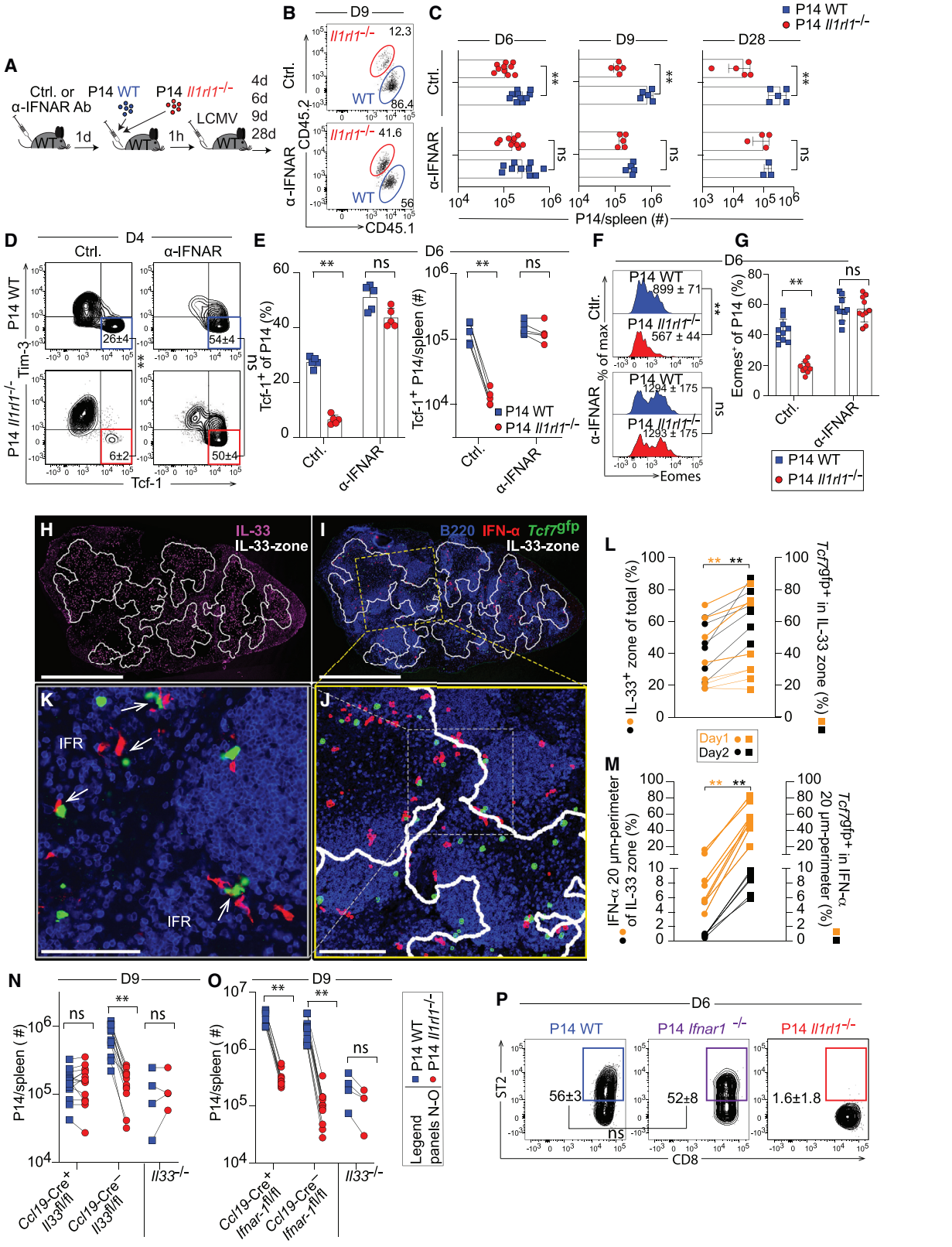

Figure 3. IFNAR blockade restores the expansion and stemness of ST2-deficient CD8+ T cells

(A–G) We treated WT (CD45.2) recipients with α-IFNAR or isotype control antibody and co-transferred equal numbers of P14 WT (CD45.1/1) and P14 *Il1rl1*$^{-/-}$ cells (CD45.1/2), followed by LCMV infection. Representative FACS plots from day 9, gated on P14 cells (B). Numbers indicate the frequency of gated populations.

(legend continued on next page)

Please cite this article in press as: Marx et al., The alarmin interleukin-33 promotes the expansion and preserves the stemness of Tcf-1$^+$ CD8$^+$ T cells in chronic viral infection, Immunity (2023), https://doi.org/10.1016/j.immuni.2023.01.029

deficiency (Figures S2H and S2I). Moreover, *Il1rl1*$^{-/-}$ P14 cells generated fewer IFN-γ single-producing and IFN-γ GzmB co-producing effector progeny on day 6 (Figures S2J and S2K), and a reduced proportion and total number of T-bet$^+$ CX3CR1$^+$ cells persisted 3 weeks into the infection (Figures S2L and S2M). Altogether these findings demonstrated that CD8$^+$SL formation but to some extent also effector cell generation was impaired in the absence of IL-33 signaling.

The analysis of *Tcf7*^{gfp} reporting by WT P14 cells that either did or did not express surface ST2 provided additional evidence for an interrelatedness of ST2 and Tcf-1. Both on day 6 and on day 14, *Tcf7*$^{gfp+}$ cells were overrepresented among those cells expressing surface ST2 (Figure 2K).

To test a potential direct IL-33 effect on *Tcf7* transcription by CD8$^+$ T cells, we activated P14 WT cells *in vitro* with cognate GP33 peptide and induced ST2 expression by adding IL-12,[45] a cytokine that exerts also *Tcf7*-repressive effects[58] (Figure 2L). The subsequent stimulation with exogenous IL-33 resulted in ~37-fold higher *Tcf7* mRNA expression levels 2 h later, identifying enhanced *Tcf7* transcription as an immediate consequence of IL-33 signaling in CD8$^+$ T cells (Figure 2M). This was also evident in elevated frequencies of Tcf-1$^+$ P14 cells and elevated Tcf-1 protein levels 6 h after IL-33 addition (Figure S2N). Taken together, these findings suggested that ST2 signaling promoted Tcf-1 expression to preserve the pool of antiviral CD8$^+$SL.

IFNAR blockade restores the expansion and stemness of ST2-deficient CD8$^+$ T cells

IFN-I signaling suppresses CD8$^+$SL differentiation[16] and our gene expression data suggested ST2 signaling attenuates IFN-I gene signatures (compare Figures 1M and S1F). Moreover, we noted that previously reported effects of IFNAR blockade on the P14 cell transcriptome[29] exhibited significant similarity to the transcriptional impact of IL-33 sensing in our datasets (Figures S3A–S3D; Table S3). In concert with published data indicating IFN-I sensing can regulate Tcf-1 expression in a CD8$^+$ T cell-intrinsic manner,[16] we found that IFNAR-deficient P14 cells (P14 *Ifnar1*$^{-/-}$ cells), when responding to LCMV challenge, retained Tcf-1 expression at a significantly higher rate than P14 WT cells (Figure S3E). Of note, P14 *Ifnar1*$^{-/-}$ cells retained Tcf-1 expression at similar levels when challenged in either WT or *Il33*-deficient hosts. These findings prompted us to investigate IFN-I effects on ST2-deficient CD8$^+$ T cells in the context of chronic viral infection. We treated recipient mice with IFNAR blocking antibodies (α-IFNAR), followed by adoptive co-transfer of P14 WT and P14 *Il1rl1*$^{-/-}$ cells and LCMV infection (Figure 3A). We found that IFNAR blockade equalized the expansion of P14 *Il1rl1*$^{-/-}$ and P14 WT cells on days 6, 9, and 28 after infection (Figures 3B and 3C). Analogously, IFNAR blockade allowed *Il1rl1*$^{-/-}$ mice to mount a polyclonal GP33-specific CD8$^+$ T cell response of normal magnitude (Figure S3F). These beneficial effects of IFNAR blockade on ST2-deficient CD8$^+$ T cell responses were not reproduced by NK cell depletion or IFN-γ blockade (Figures S3G–S3I).[59,60] Of special note, the equal expansion of P14 WT and P14 *Il1rl1*$^{-/-}$ cells under IFNAR blockade was accompanied by the cells' unimpaired differentiation into CD8$^+$SL (Figures 3D and 3E). P14 *Il1rl1*$^{-/-}$ cells yielded Tcf-1$^+$ progeny in percentages and numbers comparable to P14 WT cells (Figure 3E), and Eomes expression was also restored by IFNAR blockade (Figures 3F and 3G). CX3CR1$^+$ effector cells were reduced under IFNAR blockade yet the output from P14 WT and P14 *Il1rl1*$^{-/-}$ cells was equalized (Figure S3J).

To investigate the spatial relationship of Tcf-1-expressing P14 cells, IL-33-, and IFN-I-expressing cells in spleen, we performed immunohistochemistry on days 1 and 2 after LCMV challenge, followed by computer-assisted quantitative analyses (Figures 3H–3K). At both time points, *Tcf7*$^{gfp+}$ P14 cells were significantly enriched in the IL-33-rich zone ("IL-33 zone"; Figures 3H–3J and 3L). The detection of IFN-α-producing cells on these tissue sections evidenced a maximum on day 1, followed by a sharp decline by day 2 and a lack of detectable IFN-I producing cells on day 4 (Figure S3K), matching published serum kinetics of IFN-α.[61,62] Plasmacytoid and classical dendritic cells as well as certain macrophage subsets mediate the IFN-I response to LCMV infection,[63–66] whereas splenic IL-33 is virtually exclusively produced by FRCs.[41,42] Accordingly, our sections showed that IL-33 and IFN-α were produced by a separate set of cells (Figure S3L). Next, we defined the proximity of *Tcf7*$^{gfp+}$ P14 cells to IFN-α

Transferred cells in spleen were enumerated at the indicated time points (C). Representative FACS plots displaying Tcf-1 and Tim-3 expression on day 4 (D). Percentage of gated populations are shown as mean ± SD. Percentage and number of Tcf-1$^+$ P14 WT and P14 *Il1rl1*$^{-/-}$ CD8$^+$ T cells on day 6 (E). Representative flow cytometry plots (MFI reported as mean ± SD) and percentage of EOMES-expressing cells in spleen on day 6 (F and G).

(H–K) We transferred P14 WT *Tcf7*^{gfp} into WT recipients followed by LCMV infection. Adjacent sections from spleens collected on day 1 and day 2 were stained for IL-33 for computer-based definition of the IL-33 zone (H, zone definition transferred to aligned adjacent section in I and J) and for GFP (*Tcf7*^{gfp}), B220 and IFN-α (I–K), respectively. Computer-recognized GFP$^+$ (green) and IFN-α$^+$ (red) cells in (I) and (J) are shown with outlines. Scale bars: 500 μm in (H) and (I); 200 μm in (J); and 100 μm in (K). IFR, interfollicular region. Arrows in (K) indicate *Tcf7*^{gfp}-reporting P14 WT cells in close proximity to IFN-α$^+$ cells.

(L) The percentage of total tissue area consisting of IL-33 zone was compared with the proportion of *Tcf7*^{gfp}-positive cells in the IL-33 zone.

(M) The percentage of tissue area covered by a 20-μm perimeter around IFN-α-producing cells in the IL-33 zone was compared with the proportion of IL-33 zone-resident *Tcf7*^{gfp}-positive cells in that perimeter. Each symbol pair in (L) and (M) represents one whole spleen section from a total of 4 and 3 mice on days 1 and 2, respectively.

(N and O) We co-transferred P14 WT and P14 *Il1rl1*$^{-/-}$ cells to mice of the following genotypes and determined their expansion on day 9 after LCMV infection: mice lacking IL-33 specifically in FRCs (*CCL19*-Cre$^+$ *Il33*-fl/fl) and matching controls (*Ccl19*-Cre$^-$ *Il33*-fl/fl) as well as plain *Il33*$^{-/-}$ mice (N); mice lacking IFNAR specifically in FRCs (Ccl19-Cre$^+$ *Ifnar1*-fl/fl cells) and matching controls (*Ccl19*-Cre$^-$ *Ifnar1*-fl/fl) as well as plain *Il33*$^{-/-}$ mice (O).

(P) ST2 receptor expression was determined on adoptively transferred P14 WT and P14 *Ifnar1*$^{-/-}$ cells on day 6 after LCMV infection (P14 *Il1rl1*$^{-/-}$ cells served as negative controls).

Percentages of gated cells are shown as mean ± SD. Data in (E, F, P, and day 9/day 28 analyses in C) are representative of 2 independent experiments, day 6 in (C), (G), (N), and (O) show combined data from 2 independent experiments. Symbols in (C), (E), (G), (N), and (O) show individual mice. FACS plots are representative from 5 mice per group. Bars show means ± SD. Statistical analyses were performed by two-way ANOVA with Sidak's post-test (C–G), by one-way ANOVA with Tukey's post-test (N–P) and paired Student's t test (L and M). *$p < 0.05$; **$p < 0.01$; ns: not statistically significant.

Please also see Figure S3.

Please cite this article in press as: Marx et al., The alarmin interleukin-33 promotes the expansion and preserves the stemness of Tcf-1+ CD8+ T cells in chronic viral infection, Immunity (2023), https://doi.org/10.1016/j.immuni.2023.01.029

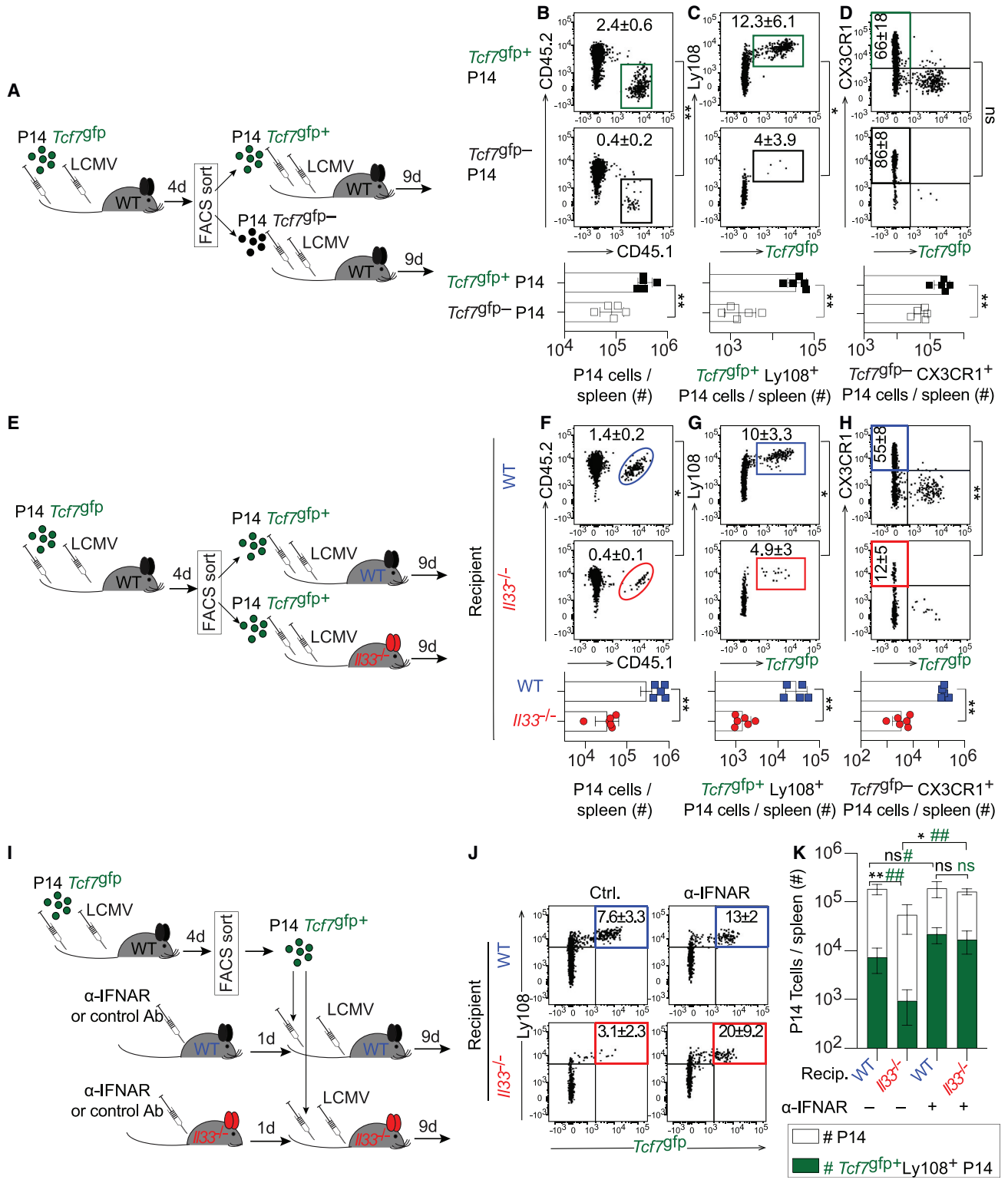

Figure 4. ST2 signals balance IFN-I effects to sustain an early Tcf-1+ CD8+SL population in chronic viral infection

(A–D) We transferred P14 WT *Tcf7*^{gfp} cells (CD45.1/1) to WT recipients followed by LCMV infection. On day 4, we sorted *Tcf7*$^{gfp+}$ and *Tcf7*$^{gfp-}$ P14 cells and re-transferred them (10^3 P14 cells/recipient) into secondary WT recipients followed by LCMV infection and analysis of spleens 9 days later. Representative FACS plots and total numbers of resulting P14 progeny (B), their co-expression of Ly108 and *Tcf7*^{gfp} (C) and of CX3CR1 with *Tcf7*^{gfp} (D).

(legend continued on next page)

Please cite this article in press as: Marx et al., The alarmin interleukin-33 promotes the expansion and preserves the stemness of Tcf-1$^+$ CD8$^+$ T cells in chronic viral infection, Immunity (2023), https://doi.org/10.1016/j.immuni.2023.01.029

producing cells in the IL-33 zone. *Tcf7*$^{gfp+}$ P14 cells where significantly enriched in a 20-μm perimeter around IFN-α producing cells of the IL-33 zone and were often found in their immediate proximity (Figures 3J, 3K, and 3M). Taken together these spatial analyses suggested that the early phase of LCMV infection offers an opportunity for CD8$^+$ T cells to integrate IFN-I and IL-33 signals.

We tested whether the restoration of P14 *Il1rl1*$^{-/-}$ cell expansion in IFNAR-blocked mice related to IFN-I effects, direct and/or indirect,[30–35] on CD8$^+$ T cells or, alternatively, might reflect an impact of IFNAR signals on IL-33 expression, its release or impaired ST2 expression by antiviral CD8$^+$ T cells. IL-33 expression by FRCs, as determined in *IL-33*^{gfp} reporter mice, was unaffected by IFNAR blockade (Figure S3N). CCL19-expressing FRCs are the main source of bioactive IL-33 fueling CD8$^+$ T cell responses.[41,42] Accordingly, the selective deletion of IL-33 from FRCs in *Ccl19-Cre*$^+$ *Il33*$^{fl/fl}$-mice annihilated the proliferative advantage of transferred P14 WT over P14 *Il1rl1*$^{-/-}$ cells, as expected (Figure 3N).[42] In contrast, the proliferative advantage of P14 WT cells was unaltered in recipients with an FRC-specific deletion of *Ifnar1* (*Ccl19-Cre*$^+$ *Ifnar1*$^{fl/fl}$ mice, Figure 3O), indicating that IL-33 release from FRCs was independent of the cells' IFNAR signaling. Finally, as already shown by,[45] *Ifnar1* deletion on P14 cells did not affect ST2 expression (Figure 3P).

Taken together these data suggested IFNAR blockade restored the expansion of the ST2-deficient Tcf-1$^+$ CD8$^+$SL subset without modulating the expression or bioavailability of IL-33 or ST2 expression levels on CD8$^+$ T cells.

ST2 signals balance IFN-I effects to sustain an early Tcf-1$^+$ CD8$^+$SL population in chronic viral infection

IL-33 release from FRC occurs in the first 3 days after LCMV challenge[42] and ST2 effects on Tcf-1 expression by CD8$^+$ T cells were evident by day 4 after infection (compare Figure 2). Next, we tested whether a Tcf-1-expressing stem-like pool of antiviral CD8$^+$ T cells could already be identified on day 4 after infection. We sorted P14 WT cells, either *Tcf7*$^{gfp+}$ or *Tcf7*$^{gfp-}$, on day 4 after infection and transferred equal numbers into individual naive recipients that were challenged with LCMV (Figure 4A). 9 days later *Tcf7*$^{gfp+}$ P14 T cells had expanded ~10-fold more than *Tcf7*$^{gfp-}$ cells (Figure 4B), and the progeny comprised ~20-fold more *Tcf7*$^{gfp+}$ Ly108$^+$ cells (Figure 4C) and more *Tcf7*$^{gfp-}$ CX3CR1$^+$ effector cells (Figure 4D). *Tcf7*^{gfp} expression reflected, therefore, an early dichotomy in the CD8$^+$ T cell population,[26] with the *Tcf7*$^{gfp+}$ subset of early CD8$^+$SL displaying superior expansion capacity and a virtually exclusive ability to produce secondary *Tcf7*$^{gfp+}$ cells.

Next, we sorted *Tcf7*$^{gfp+}$ P14 WT cells on day 4 after infection, transferred them into either WT or *Il33*$^{-/-}$ recipients and challenged them with LCMV (Figure 4E). IL-33 deficiency of these secondary recipients resulted in a ~10-fold lower overall expansion (Figure 4F), and a ~30-fold lower abundance of secondary *Tcf7*$^{gfp+}$ Ly108$^+$ stem-like P14 cell progeny (Figure 4G) and similarly curtailed *Tcf7*$^{gfp-}$ CX3CR1$^+$ effector cell yields (Figure 4H). This result indicated that early CD8$^+$SL are responsive to and depend on IL-33 signals upon antigen re-exposure for their efficient expansion and self-renewal as well as for robust effector cell generation.

Next, we assessed how IL-33 and IFN-I effects were intertwined in the population expansion and differentiation of early CD8$^+$SL. We sorted *Tcf7*$^{gfp+}$ P14 WT cells on day 4 of the response, transferred them into WT and *Il33*$^{-/-}$ secondary recipients that were either IFNAR-blocked or control-treated, and challenged them with LCMV (Figure 4I). When assessed 9 days later, IFNAR blockade restored the population expansion and, importantly, also the formation of secondary *Tcf7*$^{gfp+}$ Ly108$^+$ CD8$^+$SL progeny in IL-33-deficient hosts to the levels of WT recipients (Figures 4J and 4K). Altogether, these findings indicated that IL-33 ensured the self-renewal of early CD8$^+$SL cells when exposed to IFN-I-driven inflammation.

Early IL-33 signals impact chromatin accessibility and stemness of Tcf-1$^+$ CD8$^+$ T cells

Up to day 4 of the antiviral response, P14 *Il1rl1*$^{-/-}$ cells yielded normal numbers of Tcf-1$^+$ progeny but this population subsequently failed to expand (see Figure 2). Indeed, ST2 signaling impacted the quality of developing Tcf-1$^+$ CD8$^+$SL including these cells' self-renewing capacity (see Figure 4). Hence, we sorted P14 WT and P14 *Il1rl1*$^{-/-}$ cells, either *Tcf7*$^{gfp+}$ or *Tcf7*$^{gfp-}$, on day 4 after LCMV infection and performed genome-wide RNA expression profiling. Principal component analysis as shown in Figure 5A clustered the cells according to Tcf-1 expression rather than to genotype. Accordingly, the transcriptomes of P14 WT and P14 *Il1rl1*$^{-/-}$ cells, sorted as either *Tcf7*$^{gfp+}$ or *Tcf7*$^{gfp-}$, differed by only 10 and 9 genes, respectively (≥1.5-fold difference; FDR adjusted p value < 0.05; Table S4), and a pathway analysis performed on these datasets failed to reach statistical significance. This indicated that the dichotomous gene expression programs of the Tcf-1$^+$ and Tcf-1$^-$ CD8$^+$ T cell subsets on day 4 were largely preserved in the absence of ST2 signaling. Next, we addressed the possibility that early ST2 signals, albeit devoid of a clear impact on the day 4 transcriptome, influence the chromatin landscape of CD8$^+$SL. We sorted *Tcf7*$^{gfp+}$ P14 cells, either ST2-sufficient or -deficient, on day 4 after LCMV

(E–H) We transferred P14 WT *Tcf7*^{gfp} cells into WT mice recipients followed by LCMV infection. 4 days later, we sorted *Tcf7*$^{gfp+}$ P14 cells and re-transferred them (10^3 P14 cells/recipient) into either WT or *Il33*$^{-/-}$ secondary recipients followed by LCMV infection and analysis of spleens 9 days after re-transfer. Representative FACS plots and total numbers of resulting P14 progeny (F), their co-expression of Ly108 and *Tcf7*^{gfp} (G) and of CX3CR1 with *Tcf7*^{gfp} (H).

(I–K) We transferred P14 WT *Tcf7*^{gfp} cells into WT recipients followed by LCMV infection. 4 days later, we sorted *Tcf7*$^{gfp+}$ P14 cells and re-transferred them (10^3 P14 cells/recipient) into either WT or *Il33*$^{-/-}$ secondary recipients that had been treated 1 day before with either α-IFNAR or isotype control antibody. 9 days after challenge spleens were analyzed. Representative FACS plots show the co-expression of *Tcf7*^{gfp} and Ly108 by P14 cells (J). Total P14 cell count (white bars) and *Tcf7*$^{gfp+}$ Ly108$^+$ cells (green bars) in spleen (K).

For statistical analysis unpaired Student's t tests (B–D and F–H) and one-way ANOVA with Tukey's post-test (K) were performed. One representative of 2 independent experiments is shown in (B)–(D) and (F)–(H). Symbols in (B)–(D) and (F)–(H) show individual mice, bars in (K) the means ± SD of 5 mice per group. FACS plots are representative from 5 to 6 mice per group. Gated populations are reported as mean ± SD. $^{*,\#}p < 0.05$; $^{**,\#\#}p < 0.01$; ns: not statistically significant. * compares total P14 cells, # compares total *Tcf7*$^{gfp+}$ Ly108$^+$ P14 cells.

Please also see Figure S4.

Please cite this article in press as: Marx et al., The alarmin interleukin-33 promotes the expansion and preserves the stemness of Tcf-1+ CD8+ T cells in chronic viral infection, Immunity (2023), https://doi.org/10.1016/j.immuni.2023.01.029

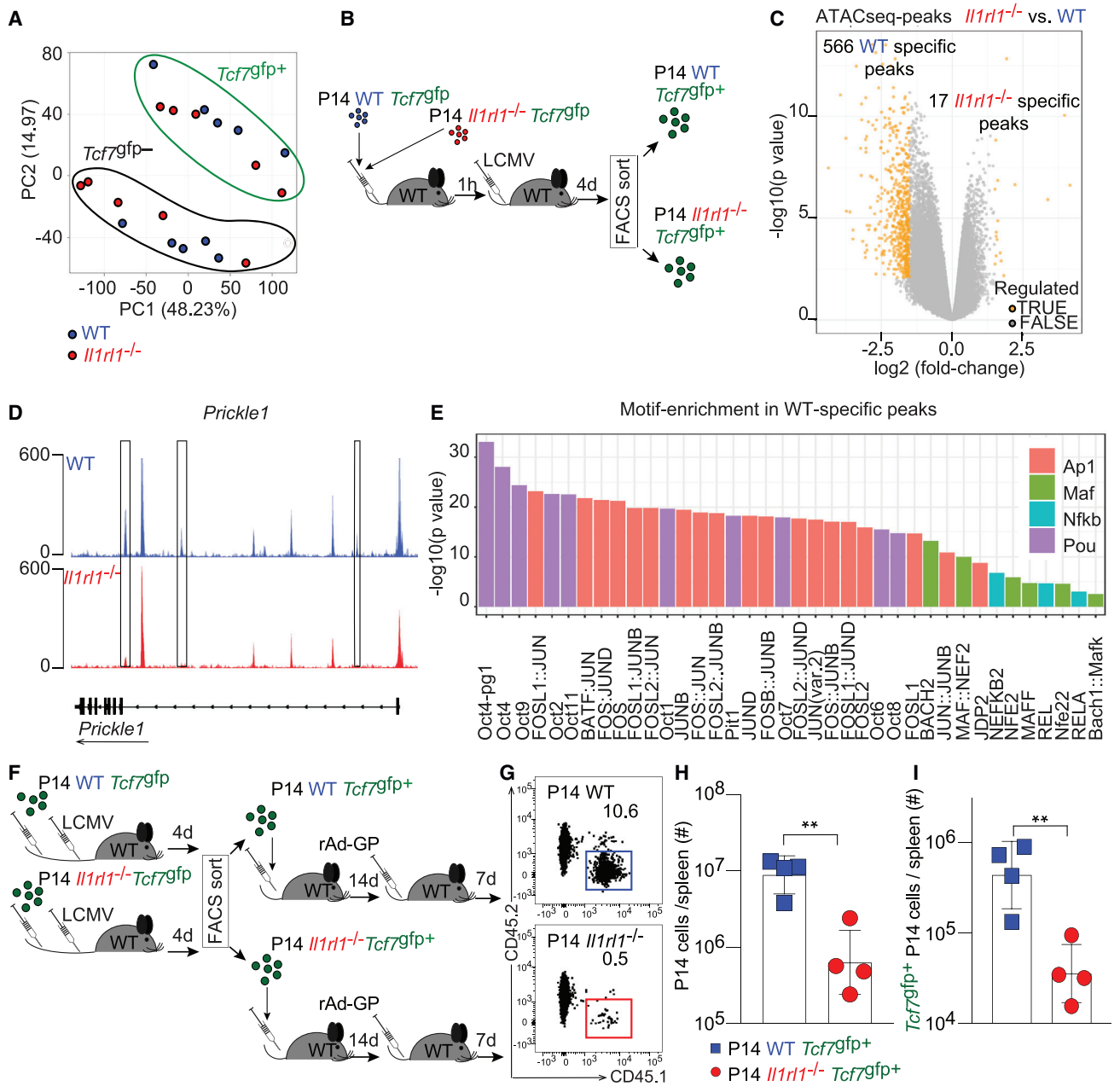

Figure 5. Early IL-33 signals impact chromatin accessibility and stemness of Tcf-1-expressing CD8+ T cells

(A) We transferred either P14 WT *Tcf7*^{gfp} or P14 *Il1rl1*$^{-/-}$ *Tcf7*^{gfp} cells into WT recipients followed by LCMV infection (analogously to Figure 2E). Principle component analysis. Each symbol represents one individual sample.

(B–E) P14 WT *Tcf7*^{gfp} and P14 *Il1rl1*$^{-/-}$ *Tcf7*^{gfp} CD8+ T cells were transferred into WT mice followed by LCMV infection. On day 4 *Tcf7*$^{gfp+}$ progeny were sorted and processed for ATAC-seq. (C) Volcano plot of peaks differentiating *Tcf7*$^{gfp+}$ P14 *Il1rl1*$^{-/-}$ from *Tcf7*$^{gfp+}$ P14 WT cells. Peaks with $\log_2$FC >1.5; FDR adjusted p value < 0.05 are highlighted in orange. (D) Normalized ATAC-seq read coverage in the *Prickle-1* locus of P14 WT *Tcf7*$^{gfp+}$ and P14 *Il1rl1*$^{-/-}$ *Tcf7*$^{gfp+}$ cells. Boxes highlight regions of differential accessibility. (E) Significantly enriched (FDR adjusted p value < 0.05) transcription factor binding motifs in peak regions specific to P14 WT *Tcf7*$^{gfp+}$ cells.

(F–I) We transferred P14 WT *Tcf7*^{gfp} and P14 *Il1rl1*$^{-/-}$ *Tcf7*^{gfp} into WT recipients followed by LCMV infection. 4 days later *Tcf7*$^{gfp+}$ cells of either genotype were sorted and 10^3 cells of each population were re-transferred into secondary WT recipients. After resting for 14 days the recipients were vaccinated with rAdGP and re-expanded P14 cells in spleen were enumerated 7 days later. Representative FACS plot show the percentage of transferred cells (G). Numbers indicate the percentage of gated cells. Total number of P14 WT *Tcf7*^{gfp} and P14 *Il1rl1*$^{-/-}$ *Tcf7*^{gfp} cell progeny (H) and of *Tcf7*$^{gfp+}$ cells among them (I).

Data in (G)–(I) are representative of 2 independent experiments, and symbols represent individual mice. Numbers indicate the mean ± SD. For statistical analysis unpaired Student's t tests were performed (H and I). **p < 0.01.

Please also see Figure S5.

Please cite this article in press as: Marx et al., The alarmin interleukin-33 promotes the expansion and preserves the stemness of Tcf-1$^+$ CD8$^+$ T cells in chronic viral infection, Immunity (2023), https://doi.org/10.1016/j.immuni.2023.01.029

infection and performed an assay for transposase accessible chromatin sequencing (ATAC-seq) (Figures 5B–5E). Among 583 differentially accessible chromatin regions (≥1.5-fold difference; FDR adjusted p value < 0.05), the vast majority, i.e., 566, were more accessible in WT *Tcf7*$^{gfp+}$ cells (Table S5), indicating that IL-33 signals broadly augmented the chromatin accessibility of Tcf-1$^+$ CD8$^+_{SL}$ cells. These effects comprised, for example, three ATAC-seq peaks in the *Prickle1* locus, which is involved in Wnt signaling and is upregulated in CD8$^+$SL[13] (Figure 5D). Two of these peaks were previously reported to differentiate stem-like CD8$^+$ T cells and exhausted CD8$^+$ T cells in chronic infection (Figure S5A). 96 of the 566 aforementioned WT-specific peaks overlapped with peaks previously found to distinguish CD8$^+$SL from exhausted CD8$^+$ T cells (p = 0.0004; Table S5).[24] In contrast, only 45 WT-specific peaks overlapped with previously reported memory T cell-specific peaks (p > 0.05), which was in line with earlier findings that CD8$^+_{SL}$ and memory T cells have rather distinct epigenetic profiles[24] (Table S5).

An analysis of transcription-factor-binding motifs indicated that peaks specific to WT cells were enriched for motifs bound by members of the Oct subclass of the POU transcription factor family or by activator protein 1 (AP-1), a heterodimer composed of proteins belonging to the c-Fos, c-Jun, ATF, and JDP families, respectively (Figure 5E). AP-1 binding accounts for ~70% of chromatin remodeling in the first hours after T cell activation,[67] whereas POU family members, most prominently Oct4 and Oct1, are key for embryonic stem cell pluripotency and for T cell memory formation, respectively.[68–71] Altogether these findings supported the conclusion that early ST2 signals left a distinct chromatin accessibility mark indicative of epigenetic priming and compatible with a profound impact on T cell activation and stemness.

To directly probe and compare the self-renewing potential of ST2-sufficient and -deficient *Tcf7*$^{gfp+}$ P14 cells, we relied on immunization with a recombinant adenovirus vector expressing the LCMV glycoprotein (rAd-GP). rAd fails to trigger the IL-33-ST2 pathway and therefore can read out CD8$^+$ T cell-intrinsic re-expansion potential without confounding IL-33 effects during the recall[37] (Figures S5B and S5C). Following established principles,[72] we designed an experimental setting, in which we sorted *Tcf7*^{gfp} P14 cells for GFP expression on day 4 after LCMV infection and transferred them to naive WT recipients (Figure S5D). After resting for 14 days in this antigen-free environment we immunized the recipients with rAd-GP and determined P14 cell progeny 7 days later. When transferring *Tcf7*$^{gfp+}$ and *Tcf7*$^{gfp-}$ P14 WT cells, the former expanded ~20-fold more, validating this experimental setting to assess and compare T cell stemness and re-expansion capacity (Figures S5E and S5F). With these tools in hands, we set out to directly probe and compare the self-renewing potential of ST2-sufficient and -deficient *Tcf7*$^{gfp+}$ P14 cells. We isolated the respective populations on day 4 after LCMV infection and transferred them to naive WT recipients (Figure 5F). 14 days later, we challenged the recipients with rAd-GP and determined P14 cell progeny 7 days thereafter. *Tcf7*$^{gfp+}$ P14 WT cells yielded ~10-fold more progeny than their ST2-deficient counterpart, indicating the stemness of *Tcf7*$^{gfp+}$ early CD8$^+$SL was impaired when lacking IL-33 signals in the first 4 days of the response (Figures 5G and 5H). Equally importantly, *Tcf7*$^{gfp+}$ P14 *Il1rl1*$^{-/-}$ cells yielded approximately 10 times less secondary *Tcf7*$^{gfp+}$ CD8$^+$SL progeny than their WT counterpart, suggesting an impaired self-renewing potential (Figure 5I). Taken together our findings indicated that IL-33 signals received during the first 4 days after chronic LCMV challenge augmented the chromatin accessibility in early CD8$^+$SL cells and profoundly improved their stemness.

DISCUSSION

This study has identified ST2 receptor signaling in the early phase of chronic viral infection as an important stemness-sustaining pathway for CD8$^+$SL. IL-33 fosters not only a high proportion of progeny cells retaining Tcf-1 expression, but it augments also the intrinsic stemness of the resulting Tcf-1-expressing CD8$^+$SL population. Apparently, not all Tcf-1$^+$ CD8$^+$ T cells are equal in terms of their self-renewal capacity, such that CD8$^+$ T cell stemness is incompletely determined by Tcf-1 expression alone. Impaired chromatin accessibility in ST2-deficient Tcf-1$^+$ CD8$^+$ T cells suggests that IL-33 impacts CD8$^+$SL stemness by an epigenetic priming event that prominently involves Oct- and AP-1-regulated genes. The context in which CD8$^+$SL evolve, namely the IL-33 signals received, impacts therefore their self-renewing capacity in continued clonal expansion as well as upon rest and subsequent rechallenge. Consequently, the reduction in number and functional impairment of CD8$^+$SL cells, when generated in the absence of IL-33 signaling, also has repercussions in its end-differentiation product, the CD8$^+$ effector cell compartment.[37,42]

The IL-33-dependence of CD8$^+$SL formation and clonal expansion is much alleviated when IFNAR signaling is blocked. It seems, therefore, that the stemness-promoting cytokine IL-33, a "damage-associated molecular pattern" (DAMP), serves to balance the differentiation-promoting effects of the prototypic antiviral "danger" response, i.e., of IFN-I. Keeping the balance between stemness and effector differentiation of CD8$^+$ T cells is a delicate task, particularly under highly inflammatory conditions of chronic viral infection,[73,74] where Tcf-1$^+$ CD8$^+$SL cells take center stage. The same may apply to other chronic infectious conditions, bacterial or parasitic, which are associated with a pronounced IFN-I gene signature.[75,76]

Given that the IL-33-dependence of CD8$^+$ T cell responses can vary greatly depending on the agent triggering them,[37,50] our findings suggest that these disparities may be due to differential IFN-I induction and/or duration of IFN-I-dependent inflammatory alterations. While the pronounced IL-33 effects on *Tcf-7* transcription detected in cultured CD8$^+$ T cells indicate that these effects operate independently of IFN-I-driven inflammation, these Tcf-1-promoting effects may well become rate limiting under highly inflammatory conditions such as in chronic microbial infection.

The identification of IL-33 as a T cell stemness-promoting factor provides a mechanistic rationale to translational ambitions of exploiting this cytokine in tumor immunotherapy.[48,49,77] Chronic IL-33 overdose can, however, have detrimental effects,[78] and preliminary observations from our laboratory indicate that exogenous IL-33 supplementation, which is well tolerated under vaccination conditions,[37,48,49,79] can have detrimental consequences in the context of chronic LCMV infection. This may not come as a surprise given that severe immunopathological

complications have been observed when other immunostimulatory cytokine supplementation or receptor blockade therapies were administered in chronic LCMV infection.[80,81] Still, IL-33 may show utility to improve the stemness of receptor-engineered T cells includin chimeric antigen receptor (CAR) T cells for therapeutic use in cancer and chronic infectious diseases. In support of this notion IL-2 therapy of chronic viral infection has been found to induce ST2 expression on antiviral CD8$^+$ T cells.[82] Moreover, IL-2 synergistically with IL-33 potentiates CAR-T cell-based tumor therapy.[83,84] The importance of ST2 signaling for CD8$^+$SL generation may also help to understand the beneficial effects of IL-33 blockade in T cell-driven immunopathological conditions such as in hemophagocytic lymphohistiocytosis and graft-versus-host disease.[85,86]

Limitations of the study

Our study has limitations in that it is confined to the LCMV infection model and mostly investigates the early phase of the antiviral CD8$^+$ T cell response. The latter focus of our work was suggested by the early release of IL-33[42] as well as by recent reports highlighting the bifurcation of stem-like and effector CD8$^+$ T cell populations in the first few days of the response.[21,26] Still, ST2 expression persisted on a subset of CD8$^+$ T cells for at least 2 weeks into chronic infection indicating that potential IL-33 effects in later phases of the response should also be studied. Elevated ST2 expression levels specifically on Tcf-1$^+$ CD8$^+$SL cells provide additional incentive for such investigations. Finally, owing to this study's focus on CD8$^+$ T cells a potential additional role of ST2 signaling in antiviral CD4 T cell responses to chronic infection remains to be addressed in future work.[87]

In summary, our study identifies the IL-33-ST2 axis as a key signaling pathway that imprints characteristic chromatin accessibility patterns in CD8$^+$SL, promotes Tcf-1 expression and stemness of CD8$^+$ T cells, and counter-balances the differentiation-promoting effects of IFN-I to warrant potent and sustainable antiviral CD8$^+$ T cell responses to chronic viral infection.

STAR★METHODS

Detailed methods are provided in the online version of this paper and include the following:

- KEY RESOURCES TABLE
- RESOURCE AVAILABILITY
  - Lead contact
  - Materials availability
  - Data and code availability
- EXPERIMENTAL MODEL AND SUBJECT DETAILS
  - Animals and ethics statement
- METHOD DETAILS
  - Viruses, virus titrations, infections and immunizations
  - Staining of cells for flow cytometric analysis
  - Cell transfer followed by next-generation RNA sequencing or ATAC sequencing and bioinformatic data analyses
  - Identification of ATAC peaks specific for stem-**like, memory and exhausted** CD8$^+$ T cells
  - Gene set enrichment analysis
  - Adoptive T cell transfer for flow cytometric analysis and re-transfer
  - *In vivo* blockade of type I interferon receptor, *in vivo* blockade of IFN-γ and NK cell depletion
  - Generation of bone marrow chimeric mice
  - Proliferation analysis
  - *In vitro* activation of P14 WT cells and exposure to IL-33
  - Immunohistochemistry and image analysis
- QUANTIFICATION AND STATISTICAL ANALYSIS

SUPPLEMENTAL INFORMATION

Supplemental information can be found online at https://doi.org/10.1016/j.immuni.2023.01.029.

ACKNOWLEDGMENTS

We wish to thank Telma Lopes, Danny Labes, Lorenzo Raeli, and Emmanuel Traunecker form the DBM flow cytometry core facility for outstanding FACS-sorting, Philippe Demougin from the Life Sciences Training Facility of the University of Basel Pharmacenter for bulk RNA-seq, and Katrin Martin for graphics. Moreover, we are grateful to the entire Experimental Virology lab for helpful discussions. Bioinformatic analysis calculations were performed at sciCORE (http://scicore.unibas.ch/) scientific computing center at University of Basel. Funding: this work was supported by the Swiss National Science Foundation (grant no. 310030_185318/1 to D.D.P., no. 310030_200898 to W.H., no. 310030_185226/1 to S.A.L., and no. CRSII3_160772/1 to D.M., S.A.L., M. Löhning, and D.D.P.), the German Research Foundation (DFG grant LO 1542/5-1 to M. Löhning), and the Willy Robert Pitzer Foundation and the Dr. Rolf M. Schwiete Foundation (both to M. Löhning).

AUTHOR CONTRIBUTIONS

A.-F.M., S.M.K., T.M.B., J.A.V., F.G., J. Fixemer, T.A.-M., P.R., W.V.B., J. Fadejeva, M.K., P.A.-D., L.S., M.C., D.T.U., D.M., D.Z., W.H., S.A.L., M. Löhning, and D.D.P. designed experiments. A.-F.M., S.M.K., T.M.B., J.A.V., T.A.-M., P.R., W.V.B., J. Fadejeva, M.K., P.A.-D., L.S., D.T.U., C.H., M. Lu, K.C., and K.S. performed experiments. A.-F.M., S.M.K., T.M.B., J.A.V., F.G., J. Fixemer, T.A.-M., P.R., W.V.B., J. Fadejeva, M.K., P.A.-D., L.S., M.C., D.T.U., D.M., D.Z., W.H., S.A.L., M. Löhning, and D.D.P. analyzed data. F.K. contributed key reagents. A.-F.M., S.M.K., and T.M.B. made the foundational observations leading to this manuscript. M. Löhning supervised the *in vitro* T cell work. A.-F.M. and D.D.P. supervised the *in vivo* work and wrote the manuscript.

DECLARATION OF INTERESTS

D.D.P. is a founder, consultant, and shareholder of Hookipa Pharma Inc. commercializing arenavirus-based vector technology, and he as well as W.V.B., S.M.K., and D.M. are listed as inventor on corresponding patents.

Received: August 11, 2022
Revised: December 22, 2022
Accepted: January 27, 2023
Published: February 20, 2023

REFERENCES

1. Schmitz, J.E., Kuroda, M.J., Santra, S., Sasseville, V.G., Simon, M.A., Lifton, M.A., Racz, P., Tenner-Racz, K., Dalesandro, M., Scallon, B.J., et al. (1999). Control of viremia in simian immunodeficiency virus infection by CD8$^+$ lymphocytes. Science *283*, 857–860. https://doi.org/10.1126/science.283.5403.857.
2. Thimme, R., Wieland, S., Steiger, C., Ghrayeb, J., Reimann, K.A., Purcell, R.H., and Chisari, F.V. (2003). CD8(+) T cells mediate viral clearance and disease pathogenesis during acute hepatitis B virus infection. J. Virol. *77*, 68–76. https://doi.org/10.1128/jvi.77.1.68-76.2003.

3. Pagès, F., Berger, A., Camus, M., Sanchez-Cabo, F., Costes, A., Molidor, R., Mlecnik, B., Kirilovsky, A., Nilsson, M., Damotte, D., et al. (2005). Effector memory T cells, early metastasis, and survival in colorectal cancer. N. Engl. J. Med. *353*, 2654–2666. https://doi.org/10.1056/NEJMoa051424.

4. Galon, J., Costes, A., Sanchez-Cabo, F., Kirilovsky, A., Mlecnik, B., Lagorce-Pagès, C., Tosolini, M., Camus, M., Berger, A., Wind, P., et al. (2006). Type, density, and location of immune cells within human colorectal tumors predict clinical outcome. Science *313*, 1960–1964. https://doi.org/10.1126/science.1129139.

5. Borrow, P., Lewicki, H., Hahn, B.H., Shaw, G.M., and Oldstone, M.B. (1994). Virus-specific CD8$^+$ cytotoxic T-lymphocyte activity associated with control of viremia in primary human immunodeficiency virus type 1 infection. J. Virol. *68*, 6103–6110. https://doi.org/10.1128/JVI.68.9.6103-6110.1994.

6. Fung-Leung, W.P., Kündig, T.M., Zinkernagel, R.M., and Mak, T.W. (1991). Immune response against lymphocytic choriomeningitis virus infection in mice without CD8$^+$ expression. J. Exp. Med. *174*, 1425–1429. https://doi.org/10.1084/jem.174.6.1425.

7. Koup, R.A., Safrit, J.T., Cao, Y., Andrews, C.A., McLeod, G., Borkowsky, W., Farthing, C., and Ho, D.D. (1994). Temporal association of cellular immune responses with the initial control of viremia in primary human immunodeficiency virus type 1 syndrome. J. Virol. *68*, 4650–4655. https://doi.org/10.1128/JVI.68.7.4650-4655.1994.

8. Matano, T., Shibata, R., Siemon, C., Connors, M., Lane, H.C., and Martin, M.A. (1998). Administration of an anti-CD8$^+$ monoclonal antibody interferes with the clearance of chimeric simian/human immunodeficiency virus during primary infections of rhesus macaques. J. Virol. *72*, 164–169. https://doi.org/10.1128/JVI.72.1.164-169.1998.

9. Moskophidis, D., Cobbold, S.P., Waldmann, H., and Lehmann-Grube, F. (1987). Mechanism of recovery from acute virus infection: treatment of lymphocytic choriomeningitis virus-infected mice with monoclonal antibodies reveals that Lyt-2$^+$ T lymphocytes mediate clearance of virus and regulate the antiviral antibody response. J. Virol. *61*, 1867–1874. https://doi.org/10.1128/JVI.61.6.1867-1874.1987.

10. Shoukry, N.H., Grakoui, A., Houghton, M., Chien, D.Y., Ghrayeb, J., Reimann, K.A., and Walker, C.M. (2003). Memory CD8$^+$ T cells are required for protection from persistent hepatitis C virus infection. J. Exp. Med. *197*, 1645–1655. https://doi.org/10.1084/jem.20030239.

11. Zhang, L., Conejo-Garcia, J.R., Katsaros, D., Gimotty, P.A., Massobrio, M., Regnani, G., Makrigiannakis, A., Gray, H., Schlienger, K., Liebman, M.N., et al. (2003). Intratumoral T cells, recurrence, and survival in epithelial ovarian cancer. N. Engl. J. Med. *348*, 203–213. https://doi.org/10.1056/NEJMoa020177.

12. Utzschneider, D.T., Charmoy, M., Chennupati, V., Pousse, L., Ferreira, D.P., Calderon-Copete, S., Danilo, M., Alfei, F., Hofmann, M., Wieland, D., et al. (2016). T cell factor 1-expressing memory-like CD8(+) T Cells Sustain the Immune Response to Chronic Viral Infections. Immunity *45*, 415–427. https://doi.org/10.1016/j.immuni.2016.07.021.

13. Im, S.J., Hashimoto, M., Gerner, M.Y., Lee, J., Kissick, H.T., Burger, M.C., Shan, Q., Hale, J.S., Lee, J., Nasti, T.H., et al. (2016). Defining CD8$^+$ T cells that provide the proliferative burst after PD-1 therapy. Nature *537*, 417–421. https://doi.org/10.1038/nature19330.

14. He, R., Hou, S., Liu, C., Zhang, A., Bai, Q., Han, M., Yang, Y., Wei, G., Shen, T., Yang, X., et al. (2016). Follicular CXCR5- expressing CD8$^+$(+) T cells curtail chronic viral infection. Nature *537*, 412–428. https://doi.org/10.1038/nature19317.

15. Leong, Y.A., Chen, Y., Ong, H.S., Wu, D., Man, K., Deleage, C., Minnich, M., Meckiff, B.J., Wei, Y., Hou, Z., et al. (2016). CXCR5(+) follicular cytotoxic T cells control viral infection in B cell follicles(+) follicular cytotoxic T cells control viral infection in B cell follicles. Nat. Immunol. *17*, 1187–1196. https://doi.org/10.1038/ni.3543.

16. Wu, T., Ji, Y., Moseman, E.A., Xu, H.C., Manglani, M., Kirby, M., Anderson, S.M., Handon, R., Kenyon, E., Elkahloun, A., et al. (2016). The TCF1-Bcl6 axis counteracts type I interferon to repress exhaustion and maintain T cell stemness. Sci Immunol. *1*, eaai8593. https://doi.org/10.1126/sciimmunol.aai8593.

17. Siddiqui, I., Schaeuble, K., Chennupati, V., Fuertes Marraco, S.A., Calderon-Copete, S., Pais Ferreira, D., Carmona, S.J., Scarpellino, L., Gfeller, D., Pradervand, S., et al. (2019). Intratumoral Tcf1+PD-1+CD8+ T Cells with Stem-like Properties Promote Tumor Control in Response to Vaccination and Checkpoint Blockade Immunotherapy. Immunity *50*, 195–211.e10. https://doi.org/10.1016/j.immuni.2018.12.021.

18. Kratchmarov, R., Magun, A.M., and Reiner, S.L. (2018). TCF1 expression marks self-renewing human CD8+(+) T cells. Blood Adv. *2*, 1685–1690. https://doi.org/10.1182/bloodadvances.2018016279.

19. Wieland, D., Kemming, J., Schuch, A., Emmerich, F., Knolle, P., Neumann-Haefelin, C., Held, W., Zehn, D., Hofmann, M., and Thimme, R. (2017). TCF1+ hepatitis C virus-specific CD8+ T cells are maintained after cessation of chronic antigen stimulation. Nat. Commun. *8*, 15050. https://doi.org/10.1038/ncomms15050.

20. Shan, Q., Hu, S., Chen, X., Danahy, D.B., Badovinac, V.P., Zang, C., and Xue, H.H. (2021). Ectopic Tcf1 expression instills a stem-like program in exhausted CD8(+) T cells to enhance viral and tumor immunity. Cell. Mol. Immunol. *18*, 1262–1277. https://doi.org/10.1038/s41423-020-0436-5.

21. Chen, Z., Ji, Z., Ngiow, S.F., Manne, S., Cai, Z., Huang, A.C., Johnson, J., Staupe, R.P., Bengsch, B., Xu, C., et al. (2019). TCF-1-Centered Transcriptional Network Drives an Effector versus Exhausted CD8$^+$ T cell-Fate Decision. Immunity *51*, 840–855.e5. https://doi.org/10.1016/j.immuni.2019.09.013.

22. Boudousquié, C., Danilo, M., Pousse, L., Jeevan-Raj, B., Angelov, G.S., Chennupati, V., Zehn, D., and Held, W. (2014). Differences in the transduction of canonical Wnt signals demarcate effector and memory CD8$^+$ T cells with distinct recall proliferation capacity. J. Immunol. *193*, 2784–2791. https://doi.org/10.4049/jimmunol.1400465.

23. Pais Ferreira, D., Silva, J.G., Wyss, T., Fuertes Marraco, S.A., Scarpellino, L., Charmoy, M., Maas, R., Siddiqui, I., Tang, L., Joyce, J.A., et al. (2020). Central memory CD8$^+$ T cells derive from stem-like Tcf7^{hi} effector cells in the absence of cytotoxic differentiation. Immunity *53*, 985–1000.e11. https://doi.org/10.1016/j.immuni.2020.09.005.

24. Jadhav, R.R., Im, S.J., Hu, B., Hashimoto, M., Li, P., Lin, J.X., Leonard, W.J., Greenleaf, W.J., Ahmed, R., and Goronzy, J.J. (2019). Epigenetic signature of PD-1$^+$ TCF1$^+$ CD8$^+$ T cells that act as resource cells during chronic viral infection and respond to PD-1 blockade. Proc. Natl. Acad. Sci. USA *116*, 14113–14118. https://doi.org/10.1073/pnas.1903520116.

25. Beltra, J.C., Manne, S., Abdel-Hakeem, M.S., Kurachi, M., Giles, J.R., Chen, Z., Casella, V., Ngiow, S.F., Khan, O., Huang, Y.J., et al. (2020). Developmental relationships of four exhausted CD8$^+$ T Cell subsets reveals underlying transcriptional and epigenetic landscape control mechanisms. Immunity *52*, 825–841.e8. https://doi.org/10.1016/j.immuni.2020.04.014.

26. Utzschneider, D.T., Gabriel, S.S., Chisanga, D., Gloury, R., Gubser, P.M., Vasanthakumar, A., Shi, W., and Kallies, A. (2020). Early precursor T cells establish and propagate T cell exhaustion in chronic infection. Nat. Immunol. *21*, 1256–1266. https://doi.org/10.1038/s41590-020-0760-z.

27. Kim, M.V., Ouyang, W., Liao, W., Zhang, M.Q., and Li, M.O. (2013). The transcription factor FoxO1 controls central-memory CD8$^+$ T cell responses to infection. Immunity *39*, 286–297. https://doi.org/10.1016/j.immuni.2013.07.013.

28. Alfei, F., Kanev, K., Hofmann, M., Wu, M., Ghoneim, H.E., Roelli, P., Utzschneider, D.T., von Hoesslin, M., Cullen, J.G., Fan, Y., et al. (2019). TOX reinforces the phenotype and longevity of exhausted T cells in chronic viral infection. Nature *571*, 265–269. https://doi.org/10.1038/s41586-019-1326-9.

29. Huang, Z., Zak, J., Pratumchai, I., Shaabani, N., Vartabedian, V.F., Nguyen, N., Wu, T., Xiao, C., and Teijaro, J.R. (2019). IL-27 promotes the expansion of self-renewing CD8(+) T cells in persistent viral infection. J. Exp. Med. *216*, 1791–1808. https://doi.org/10.1084/jem.20190173.

30. Crouse, J., Kalinke, U., and Oxenius, A. (2015). Regulation of antiviral T cell responses by type I interferons. Nat. Rev. Immunol. *15*, 231–242. https://doi.org/10.1038/nri3806.

31. Le Bon, A., Etchart, N., Rossmann, C., Ashton, M., Hou, S., Gewert, D., Borrow, P., and Tough, D.F. (2003). Cross-priming of CD8$^+$ T cells stimulated by virus-induced type I interferon. Nat. Immunol. *4*, 1009–1015. https://doi.org/10.1038/ni978.

32. Welsh, R.M., Bahl, K., Marshall, H.D., and Urban, S.L. (2012). Type 1 interferons and antiviral CD8$^+$ T-cell responses. PLOS Pathog. *8*, e1002352. https://doi.org/10.1371/journal.ppat.1002352.

33. Curtsinger, J.M., Valenzuela, J.O., Agarwal, P., Lins, D., and Mescher, M.F. (2005). Type I IFNs provide a third signal to CD8$^+$ T cells to stimulate clonal expansion and differentiation. J. Immunol. *174*, 4465–4469. https://doi.org/10.4049/jimmunol.174.8.4465.

34. Keppler, S.J., Rosenits, K., Koegl, T., Vucikuja, S., and Aichele, P. (2012). Signal 3 cytokines as modulators of primary immune responses during infections: the interplay of type I IFN and IL-12 in CD8$^+$ T cell responses. PLoS One *7*, e40865. https://doi.org/10.1371/journal.pone.0040865.

35. Wiesel, M., Crouse, J., Bedenikovic, G., Sutherland, A., Joller, N., and Oxenius, A. (2012). Type-I IFN drives the differentiation of short-lived effector CD8$^+$ T cells in vivo. Eur. J. Immunol. *42*, 320–329. https://doi.org/10.1002/eji.201142091.

36. Schmitz, J., Owyang, A., Oldham, E., Song, Y., Murphy, E., McClanahan, T.K., Zurawski, G., Moshrefi, M., Qin, J., Li, X., et al. (2005). IL-33, an interleukin-1-like cytokine that signals via the IL-1 receptor-related protein ST2 and induces T helper type 2-associated cytokines. Immunity *23*, 479–490. https://doi.org/10.1016/j.immuni.2005.09.015.

37. Bonilla, W.V., Fröhlich, A., Senn, K., Kallert, S., Fernandez, M., Johnson, S., Kreutzfeldt, M., Hegazy, A.N., Schrick, C., Fallon, P.G., et al. (2012). The alarmin interleukin-33 drives protective antiviral CD8(+) T cell responses. Science *335*, 984–989. https://doi.org/10.1126/science.1215418.

38. Yang, Q., Li, G., Zhu, Y., Liu, L., Chen, E., Turnquist, H., Zhang, X., Finn, O.J., Chen, X., and Lu, B. (2011). IL-33 synergizes with TCR and IL-12 signaling to promote the effector function of CD8$^+$ T cells. Eur. J. Immunol. *41*, 3351–3360. https://doi.org/10.1002/eji.201141629.

39. Li, C., Yu, T., Shi, X., and Yu, J. (2022). Interleukin-33 reinvigorates antiviral function of viral-specific CD8$^+$ T Cells in Chronic Hepatitis B Virus Infection. Viral Immunol. *35*, 41–49. https://doi.org/10.1089/vim.2021.0140.

40. Peine, M., Marek, R.M., and Löhning, M. (2016). IL-33 in T cell differentiation, function, and immune homeostasis. Trends Immunol. *37*, 321–333. https://doi.org/10.1016/j.it.2016.03.007.

41. Kallert, S.M., Darbre, S., Bonilla, W.V., Kreutzfeldt, M., Page, N., Müller, P., Kreuzaler, M., Lu, M., Favre, S., Kreppel, F., et al. (2017). Replicating viral vector platform exploits alarmin signals for potent CD8(+) T cell-mediated tumour immunotherapy. Nat. Commun. *8*, 15327. https://doi.org/10.1038/ncomms15327.

42. Aparicio-Domingo, P., Cannelle, H., Buechler, M.B., Nguyen, S., Kallert, S.M., Favre, S., Alouche, N., Papazian, N., Ludewig, B., Cupedo, T., et al. (2021). Fibroblast-derived IL-33 is dispensable for lymph node homeostasis but critical for CD8$^+$ T-cell responses to acute and chronic viral infection. Eur. J. Immunol. *51*, 76–90. https://doi.org/10.1002/eji.201948413.

43. Tominaga, S. (1989). A putative protein of a growth specific cDNA from BALB/c-3T3 cells is highly similar to the extracellular portion of mouse interleukin 1 receptor. FEBS Lett. *258*, 301–304. https://doi.org/10.1016/0014-5793(89)81679-5.

44. Löhning, M., Stroehmann, A., Coyle, A.J., Grogan, J.L., Lin, S., Gutierrez-Ramos, J.C., Levinson, D., Radbruch, A., and Kamradt, T. (1998). T1/ST2 is preferentially expressed on murine Th2 cells, independent of interleukin 4, interleukin 5, and interleukin 10, and important for Th2 effector function. Proc. Natl. Acad. Sci. USA *95*, 6930–6935. https://doi.org/10.1073/pnas.95.12.6930.

45. Baumann, C., Fröhlich, A., Brunner, T.M., Holecska, V., Pinschewer, D.D., and Löhning, M. (2019). Memory CD8$^+$ T cell protection from viral reinfection depends on interleukin-33 alarmin signals. Front. Immunol. *10*, 1833. https://doi.org/10.3389/fimmu.2019.01833.

46. Ring, S.S., Cupovic, J., Onder, L., Lütge, M., Perez-Shibayama, C., Gil-Cruz, C., Scandella, E., De Martin, A., Mörbe, U., Hartmann, F., et al. (2021). Viral vector-mediated reprogramming of the fibroblastic tumor stroma sustains curative melanoma treatment. Nat. Commun. *12*, 4734. https://doi.org/10.1038/s41467-021-25057-w.

47. Dominguez, D., Ye, C., Geng, Z., Chen, S., Fan, J., Qin, L., Long, A., Wang, L., Zhang, Z., Zhang, Y., et al. (2017). Exogenous IL-33 restores dendritic cell activation and maturation in established cancer. J. Immunol. *198*, 1365–1375. https://doi.org/10.4049/jimmunol.1501399.

48. Villarreal, D.O., Wise, M.C., Walters, J.N., Reuschel, E.L., Choi, M.J., Obeng-Adjei, N., Yan, J., Morrow, M.P., and Weiner, D.B. (2014). Alarmin IL-33 acts as an immunoadjuvant to enhance antigen-specific tumor immunity. Cancer Res. *74*, 1789–1800. https://doi.org/10.1158/0008-5472.CAN-13-2729.

49. Villarreal, D.O., Svoronos, N., Wise, M.C., Shedlock, D.J., Morrow, M.P., Conejo-Garcia, J.R., and Weiner, D.B. (2015). Molecular adjuvant IL-33 enhances the potency of a DNA vaccine in a lethal challenge model. Vaccine *33*, 4313–4320. https://doi.org/10.1016/j.vaccine.2015.03.086.

50. Bonilla, W.V., Kirchhammer, N., Marx, A.F., Kallert, S.M., Krzyzaniak, M.A., Lu, M., Darbre, S., Schmidt, S., Raguz, J., Berka, U., et al. (2021). Heterologous arenavirus vector prime-boost overrules self-tolerance for efficient tumor-specific CD8$^+$ T cell attack. Cell Rep. Med. *2*, 100209. https://doi.org/10.1016/j.xcrm.2021.100209.

51. Pircher, H., Bürki, K., Lang, R., Hengartner, H., and Zinkernagel, R.M. (1989). Tolerance induction in double specific T-cell receptor transgenic mice varies with antigen. Nature *342*, 559–561.

52. Miller, B.C., Sen, D.R., Al Abosy, R., Bi, K., Virkud, Y.V., LaFleur, M.W., Yates, K.B., Lako, A., Felt, K., Naik, G.S., et al. (2019). Subsets of exhausted CD8+(+) T cells differentially mediate tumor control and respond to checkpoint blockade. Nat. Immunol. *20*, 326–336. https://doi.org/10.1038/s41590-019-0312-6.

53. Yao, C., Sun, H.W., Lacey, N.E., Ji, Y., Moseman, E.A., Shih, H.Y., Heuston, E.F., Kirby, M., Anderson, S., Cheng, J., et al. (2019). Single-cell RNA-seq reveals TOX as a key regulator of CD8+(+) T cell persistence in chronic infection. Nat. Immunol. *20*, 890–901. https://doi.org/10.1038/s41590-019-0403-4.

54. Willinger, T., Freeman, T., Herbert, M., Hasegawa, H., McMichael, A.J., and Callan, M.F. (2006). Human naive CD8$^+$ T cells down-regulate expression of the WNT pathway transcription factors lymphoid enhancer binding factor 1 and transcription factor 7 (T cell factor-1) following antigen encounter in vitro and in vivo. J. Immunol. *176*, 1439–1446. https://doi.org/10.4049/jimmunol.176.3.1439.

55. Banerjee, A., Gordon, S.M., Intlekofer, A.M., Paley, M.A., Mooney, E.C., Lindsten, T., Wherry, E.J., and Reiner, S.L. (2010). Cutting edge: the transcription factor eomesodermin enables CD8$^+$ T cells to compete for the memory cell niche. J. Immunol. *185*, 4988–4992. https://doi.org/10.4049/jimmunol.1002042.

56. Hudson, W.H., Gensheimer, J., Hashimoto, M., Wieland, A., Valanparambil, R.M., Li, P., Lin, J.X., Konieczny, B.T., Im, S.J., Freeman, G.J., et al. (2019). Proliferating transitory T cells with an effector-like transcriptional signature emerge from PD-1+ stem-like CD8+ T cells during chronic infection(+) stem-like CD8(+) T cells during chronic infection. Immunity *51*, 1043–1058.e4. https://doi.org/10.1016/j.immuni.2019.11.002.

57. Zander, R., Schauder, D., Xin, G., Nguyen, C., Wu, X., Zajac, A., and Cui, W. (2019). CD4+ T Cell Help Is Required for the Formation of a Cytolytic CD8+ T Cell Subset that Protects against Chronic Infection and Cancer. Immunity *51*, 1028–1042.e4. https://doi.org/10.1016/j.immuni.2019.10.009.

58. Danilo, M., Chennupati, V., Silva, J.G., Siegert, S., and Held, W. (2018). Suppression of Tcf1 by inflammatory cytokines facilitates effector

CD8$^+$ T cell differentiation. Cell Rep. *22*, 2107–2117. https://doi.org/10.1016/j.celrep.2018.01.072.

59. Crouse, J., Bedenikovic, G., Wiesel, M., Ibberson, M., Xenarios, I., Von Laer, D., Kalinke, U., Vivier, E., Jonjic, S., and Oxenius, A. (2014). Type I interferons protect T cells against NK cell attack mediated by the activating receptor NCR1. Immunity *40*, 961–973. https://doi.org/10.1016/j.immuni.2014.05.003.

60. Xu, H.C., Grusdat, M., Pandyra, A.A., Polz, R., Huang, J., Sharma, P., Deenen, R., Köhrer, K., Rahbar, R., Diefenbach, A., et al. (2014). Type I interferon protects antiviral CD8$^+$ T cells from NK cell cytotoxicity. Immunity *40*, 949–960. https://doi.org/10.1016/j.immuni.2014.05.004.

61. Fallet, B., Narr, K., Ertuna, Y.I., Remy, M., Sommerstein, R., Cornille, K., Kreutzfeldt, M., Page, N., Zimmer, G., Geier, F., et al. (2016). Interferon-driven deletion of antiviral B cells at the onset of chronic infection. Sci. Immunol. *1*. https://doi.org/10.1126/sciimmunol.aah6817.

62. Teijaro, J.R., Ng, C., Lee, A.M., Sullivan, B.M., Sheehan, K.C., Welch, M., Schreiber, R.D., de la Torre, J.C., and Oldstone, M.B. (2013). Persistent LCMV infection is controlled by blockade of type I interferon signaling. Science *340*, 207–211. https://doi.org/10.1126/science.1235214.

63. Montoya, M., Edwards, M.J., Reid, D.M., and Borrow, P. (2005). Rapid activation of spleen dendritic cell subsets following lymphocytic choriomeningitis virus infection of mice: analysis of the involvement of type 1 IFN. J. Immunol. *174*, 1851–1861. https://doi.org/10.4049/jimmunol.174.4.1851.

64. Diebold, S.S., Montoya, M., Unger, H., Alexopoulou, L., Roy, P., Haswell, L.E., Al-Shamkhani, A., Flavell, R., Borrow, P., and Reis e Sousa, C. (2003). Viral infection switches non-plasmacytoid dendritic cells into high interferon producers. Nature *424*, 324–328. https://doi.org/10.1038/nature01783.

65. Jung, A., Kato, H., Kumagai, Y., Kumar, H., Kawai, T., Takeuchi, O., and Akira, S. (2008). Lymphocytoid choriomeningitis virus activates plasmacytoid dendritic cells and induces a cytotoxic T-cell response via MyD88. J. Virol. *82*, 196–206. https://doi.org/10.1128/JVI.01640-07.

66. Shaabani, N., Khairnar, V., Duhan, V., Zhou, F., Tur, R.F., Häussinger, D., Recher, M., Tumanov, A.V., Hardt, C., Pinschewer, D., et al. (2016). Two separate mechanisms of enforced viral replication balance innate and adaptive immune activation. J. Autoimmun. *67*, 82–89. https://doi.org/10.1016/j.jaut.2015.10.004.

67. Yukawa, M., Jagannathan, S., Vallabh, S., Kartashov, A.V., Chen, X., Weirauch, M.T., and Barski, A. (2020). AP-1 activity induced by co-stimulation is required for chromatin opening during T cell activation. J. Exp. Med. *217*, e20182009. https://doi.org/10.1084/jem.20182009.

68. Kim, K.P., Wu, Y., Yoon, J., Adachi, K., Wu, G., Velychko, S., MacCarthy, C.M., Shin, B., Röpke, A., Arauzo-Bravo, M.J., et al. (2020). Reprogramming competence of OCT factors is determined by transactivation domains. Sci. Adv. *6*, eaaz7364. https://doi.org/10.1126/sciadv.aaz7364.

69. Takahashi, K., and Yamanaka, S. (2006). Induction of pluripotent stem cells from mouse embryonic and adult fibroblast cultures by defined factors. Cell *126*, 663–676. https://doi.org/10.1016/j.cell.2006.07.024.

70. Hayashi, H., Arao, T., Togashi, Y., Kato, H., Fujita, Y., De Velasco, M.A., Kimura, H., Matsumoto, K., Tanaka, K., Okamoto, I., et al. (2015). The OCT4 pseudogene POU5F1B is amplified and promotes an aggressive phenotype in gastric cancer. Oncogene *34*, 199–208. https://doi.org/10.1038/onc.2013.547.

71. Shakya, A., Goren, A., Shalek, A., German, C.N., Snook, J., Kuchroo, V.K., Yosef, N., Chan, R.C., Regev, A., Williams, M.A., and Tantin, D. (2015). Oct1 and OCA-B are selectively required for CD4 memory T cell function. J. Exp. Med. *212*, 2115–2131. https://doi.org/10.1084/jem.20150363.

72. Borsa, M., Barnstorf, I., Baumann, N.S., Pallmer, K., Yermanos, A., Gräbnitz, F., Barandun, N., Hausmann, A., Sandu, I., Barral, Y., et al. (2019). Modulation of asymmetric cell division as a mechanism to boost CD8(+) T cell memory. Sci. Immunol. *4*, eaav1730. https://doi.org/10.1126/sciimmunol.aav1730.

73. Bolen, C.R., Robek, M.D., Brodsky, L., Schulz, V., Lim, J.K., Taylor, M.W., and Kleinstein, S.H. (2013). The blood transcriptional signature of chronic hepatitis C virus is consistent with an ongoing interferon-mediated antiviral response. J. Interferon Cytokine Res. *33*, 15–23. https://doi.org/10.1089/jir.2012.0037.

74. Mandl, J.N., Barry, A.P., Vanderford, T.H., Kozyr, N., Chavan, R., Klucking, S., Barrat, F.J., Coffman, R.L., Staprans, S.I., and Feinberg, M.B. (2008). Divergent TLR7 and TLR9 signaling and type I interferon production distinguish pathogenic and nonpathogenic AIDS virus infections. Nat. Med. *14*, 1077–1087. https://doi.org/10.1038/nm.1871.

75. Rocha, B.C., Marques, P.E., Leoratti, F.M.S., Junqueira, C., Pereira, D.B., Antonelli, L.R.D.V., Menezes, G.B., Golenbock, D.T., and Gazzinelli, R.T. (2015). Type I interferon transcriptional signature in neutrophils and low-density granulocytes are associated with tissue damage in malaria. Cell Rep. *13*, 2829–2841. https://doi.org/10.1016/j.celrep.2015.11.055.

76. Krupka, M., Seydel, K., Feintuch, C.M., Yee, K., Kim, R., Lin, C.Y., Calder, R.B., Petersen, C., Taylor, T., and Daily, J. (2012). Mild Plasmodium falciparum malaria following an episode of severe malaria is associated with induction of the interferon pathway in Malawian children. Infect. Immun. *80*, 1150–1155. https://doi.org/10.1128/IAI.06008-11.

77. He, H., Shi, L., Meng, D., Zhou, H., Ma, J., Wu, Y., Wu, Y., Gu, Y., Xie, W., Zhang, J., et al. (2021). PD-1 blockade combined with IL-33 enhances the antitumor immune response in a type-1 lymphocyte-mediated manner. Cancer Treat. Res. Commun. *28*, 100379. https://doi.org/10.1016/j.ctarc.2021.100379.

78. Bessa, J., Meyer, C.A., de Vera Mudry, M.C., Schlicht, S., Smith, S.H., Iglesias, A., and Cote-Sierra, J. (2014). Altered subcellular localization of IL-33 leads to non-resolving lethal inflammation. J. Autoimmun. *55*, 33–41. https://doi.org/10.1016/j.jaut.2014.02.012.

79. Villarreal, D.O., and Weiner, D.B. (2015). IL-33 isoforms: their future as vaccine adjuvants? Expert Rev. Vaccines *14*, 489–492. https://doi.org/10.1586/14760584.2015.1011135.

80. Yi, J.S., Du, M., and Zajac, A.J. (2009). A vital role for interleukin-21 in the control of a chronic viral infection. Science *324*, 1572–1576. https://doi.org/10.1126/science.1175194.

81. Frebel, H., Nindl, V., Schuepbach, R.A., Braunschweiler, T., Richter, K., Vogel, J., Wagner, C.A., Loffing-Cueni, D., Kurrer, M., Ludewig, B., et al. (2012). Programmed death 1 protects from fatal circulatory failure during systemic virus infection of mice. J. Exp. Med. *209*, 2485–2499. https://doi.org/10.1084/jem.20121015.

82. Hashimoto, M., Araki, K., Cardenas, M.A., Li, P., Jadhav, R.R., Kissick, H.T., Hudson, W.H., McGuire, D.J., Obeng, R.C., Wieland, A., et al. (2022). PD-1 combination therapy with IL-2 modifies CD8(+) T cell exhaustion program. Nature *610*, 173–181. https://doi.org/10.1038/s41586-022-05257-0.

83. Brog, R.A., Ferry, S.L., Schiebout, C.T., Messier, C.M., Cook, W.J., Abdullah, L., Zou, J., Kumar, P., Sentman, C.L., Frost, H.R., and Huang, Y.H. (2022). Superkine IL2 and IL33 armored CAR T cells reshape the tumor microenvironment and reduce growth of multiple solid tumors. Cancer Immunol. Res. *10*, 962–977. https://doi.org/10.1158/2326-6066.CIR-21-0536.

84. Corria-Osorio, J., S.J.C., Stefanidis, E., Andreatta, M., Muller, T., Ortiz-Miranda, Y., Seijo, B., Castro, W., Jimenez-Luna, C., Scarpellino, L., et al. (2022). Orthogonal gene engineering enables CD8$^+$ T cells to control tumors through a novel PD-1$^+$TOX-indifferent synthetic effector state. Preprint at bioRxiv. https://doi.org/10.1101/2022.02.18.481059.

85. Rood, J.E., Burn, T.N., Neal, V., Chu, N., and Behrens, E.M. (2018). Disruption of IL-33 signaling limits early CD8$^+$ T cell effector function leading to exhaustion in murine hemophagocytic lymphohistiocytosis. Front. Immunol. *9*, 2642. https://doi.org/10.3389/fimmu.2018.02642.

86. Reichenbach, D.K., Schwarze, V., Matta, B.M., Tkachev, V., Lieberknecht, E., Liu, Q., Koehn, B.H., Pfeifer, D., Taylor, P.A., Prinz, G., et al. (2015). The IL-33/ST2 axis augments effector T-cell responses

during acute GVHD. Blood *125*, 3183–3192. https://doi.org/10.1182/blood-2014-10-606830.

87. Baumann, C., Bonilla, W.V., Fröhlich, A., Helmstetter, C., Peine, M., Hegazy, A.N., Pinschewer, D.D., and Löhning, M. (2015). T-bet- and STAT4-dependent IL-33 receptor expression directly promotes antiviral Th1 cell responses. Proc. Natl. Acad. Sci. USA *112*, 4056–4061. https://doi.org/10.1073/pnas.1418549112.

88. Battegay, M., Cooper, S., Althage, A., Bänziger, J., Hengartner, H., and Zinkernagel, R.M. (1991). Quantification of lymphocytic choriomeningitis virus with an immunological focus assay in 24- or 96-well plates. J. Virol. Methods *33*, 191–198. https://doi.org/10.1016/0166-0934(91)90018-U.

89. Ahmed, R., Salmi, A., Butler, L.D., Chiller, J.M., and Oldstone, M.B. (1984). Selection of genetic variants of lymphocytic choriomeningitis virus in spleens of persistently infected mice. Role in suppression of cytotoxic T lymphocyte response and viral persistence. J. Exp. Med. *160*, 521–540. https://doi.org/10.1084/jem.160.2.521.

90. Townsend, M.J., Fallon, P.G., Matthews, D.J., Jolin, H.E., and McKenzie, A.N. (2000). T1/ST2-deficient mice demonstrate the importance of T1/ST2 in developing primary T helper cell type 2 responses. J. Exp. Med. *191*, 1069–1076. https://doi.org/10.1084/jem.191.6.1069.

91. Oboki, K., Ohno, T., Kajiwara, N., Arae, K., Morita, H., Ishii, A., Nambu, A., Abe, T., Kiyonari, H., Matsumoto, K., et al. (2010). IL-33 is a crucial amplifier of innate rather than acquired immunity. Proc. Natl. Acad. Sci. USA *107*, 18581–18586. https://doi.org/10.1073/pnas.1003059107.

92. Müller, U., Steinhoff, U., Reis, L.F., Hemmi, S., Pavlovic, J., Zinkernagel, R.M., and Aguet, M. (1994). Functional role of type I and type II interferons in antiviral defense. Science *264*, 1918–1921. https://doi.org/10.1126/science.8009221.

93. Chai, Q., Onder, L., Scandella, E., Gil-Cruz, C., Perez-Shibayama, C., Cupovic, J., Danuser, R., Sparwasser, T., Luther, S.A., Thiel, V., et al. (2013). Maturation of lymph node fibroblastic reticular cells from myofibroblastic precursors is critical for antiviral immunity. Immunity *38*, 1013–1024. https://doi.org/10.1016/j.immuni.2013.03.012.

94. Prinz, M., Schmidt, H., Mildner, A., Knobeloch, K.P., Hanisch, U.K., Raasch, J., Merkler, D., Detje, C., Gutcher, I., Mages, J., et al. (2008). Distinct and nonredundant in vivo functions of IFNAR on myeloid cells limit autoimmunity in the central nervous system. Immunity *28*, 675–686. https://doi.org/10.1016/j.immuni.2008.03.011.

95. Chen, W.Y., Hong, J., Gannon, J., Kakkar, R., and Lee, R.T. (2015). Myocardial pressure overload induces systemic inflammation through endothelial cell IL-33. Proc. Natl. Acad. Sci. USA *112*, 7249–7254. https://doi.org/10.1073/pnas.1424236112.

96. Dobin, A., Davis, C.A., Schlesinger, F., Drenkow, J., Zaleski, C., Jha, S., Batut, P., Chaisson, M., and Gingeras, T.R. (2013). STAR: ultrafast universal RNA-seq aligner. Bioinformatics *29*, 15–21. https://doi.org/10.1093/bioinformatics/bts635.

97. Langmead, B., and Salzberg, S.L. (2012). Fast gapped-read alignment with Bowtie 2. Nat. Methods *9*, 357–359. https://doi.org/10.1038/nmeth.1923.

98. Zhang, Y., Liu, T., Meyer, C.A., Eeckhoute, J., Johnson, D.S., Bernstein, B.E., Nusbaum, C., Myers, R.M., Brown, M., Li, W., et al. (2008). Model-based analysis of ChIP-Seq (MACS). Genome Biol. *9*, R137. https://doi.org/10.1186/gb-2008-9-9-r137.

99. Li, H., Handsaker, B., Wysoker, A., Fennell, T., Ruan, J., Homer, N., Marth, G., Abecasis, G., and Durbin, R.; 1000 Genome Project Data Processing Subgroup (2009). The Sequence Alignment/Map format and SAMtools. Bioinformatics *25*, 2078–2079. https://doi.org/10.1093/bioinformatics/btp352.

100. Huber, W., Carey, V.J., Gentleman, R., Anders, S., Carlson, M., Carvalho, B.S., Bravo, H.C., Davis, S., Gatto, L., Girke, T., et al. (2015). Orchestrating high-throughput genomic analysis with Bioconductor. Nat. Methods *12*, 115–121. https://doi.org/10.1038/nmeth.3252.

101. McCarthy, D.J., Chen, Y., and Smyth, G.K. (2012). Differential expression analysis of multifactor RNA-Seq experiments with respect to biological variation. Nucleic Acids Res. *40*, 4288–4297. https://doi.org/10.1093/nar/gks042.

102. Gu, Z., Eils, R., and Schlesner, M. (2016). Complex heatmaps reveal patterns and correlations in multidimensional genomic data. Bioinformatics *32*, 2847–2849. https://doi.org/10.1093/bioinformatics/btw313.

103. Corces, M.R., Trevino, A.E., Hamilton, E.G., Greenside, P.G., Sinnott-Armstrong, N.A., Vesuna, S., Satpathy, A.T., Rubin, A.J., Montine, K.S., Wu, B., et al. (2017). An improved ATAC-seq protocol reduces background and enables interrogation of frozen tissues. Nat. Methods *14*, 959–962. https://doi.org/10.1038/nmeth.4396.

104. Lun, A.T., and Smyth, G.K. (2016). csaw: a bioconductor package for differential binding analysis of ChIP-seq data using sliding windows. Nucleic Acids Res. *44*, e45. https://doi.org/10.1093/nar/gkv1191.

105. Hahne, F., and Ivanek, R. (2016). Visualizing genomic data using gviz and bioconductor. Methods Mol. Biol. *1418*, 335–351. https://doi.org/10.1007/978-1-4939-3578-9_16.

106. Subramanian, A., Tamayo, P., Mootha, V.K., Mukherjee, S., Ebert, B.L., Gillette, M.A., Paulovich, A., Pomeroy, S.L., Golub, T.R., Lander, E.S., et al. (2005). Gene set enrichment analysis: a knowledge-based approach for interpreting genome-wide expression profiles. Proc. Natl. Acad. Sci. USA *102*, 15545–15550. https://doi.org/10.1073/pnas.0506580102.

107. Wu, T., Hu, E., Xu, S., Chen, M., Guo, P., Dai, Z., Feng, T., Zhou, L., Tang, W., Zhan, L., et al. (2021). clusterProfiler 4.0: A universal enrichment tool for interpreting omics data. Innovation (Camb) *2*, 100141. https://doi.org/10.1016/j.xinn.2021.100141.

108. Lachmann, A., Torre, D., Keenan, A.B., Jagodnik, K.M., Lee, H.J., Wang, L., Silverstein, M.C., and Ma'ayan, A. (2018). Massive mining of publicly available RNA-seq data from human and mouse. Nat. Commun. *9*, 1366. https://doi.org/10.1038/s41467-018-03751-6.

109. Love, M.I., Huber, W., and Anders, S. (2014). Moderated estimation of fold change and dispersion for RNA-seq data with DESeq2. Genome Biol. *15*, 550. https://doi.org/10.1186/s13059-014-0550-8.

110. Hao, Y., Hao, S., Andersen-Nissen, E., Mauck, W.M., 3rd, Zheng, S., Butler, A., Lee, M.J., Wilk, A.J., Darby, C., Zager, M., et al. (2021). Integrated analysis of multimodal single-cell data. Cell *184*, 3573–3587.e29. https://doi.org/10.1016/j.cell.2021.04.048.

111. Hafemeister, C., and Satija, R. (2019). Normalization and variance stabilization of single-cell RNA-seq data using regularized negative binomial regression. Genome Biol. *20*, 296. https://doi.org/10.1186/s13059-019-1874-1.

112. Blattman, J.N., Antia, R., Sourdive, D.J., Wang, X., Kaech, S.M., Murali-Krishna, K., Altman, J.D., and Ahmed, R. (2002). Estimating the precursor frequency of naive antigen-specific CD8$^+$ T cells. J. Exp. Med. *195*, 657–664. https://doi.org/10.1084/jem.20001021.

Please cite this article in press as: Marx et al., The alarmin interleukin-33 promotes the expansion and preserves the stemness of Tcf-1^{+} CD8^{+} T cells in chronic viral infection, Immunity (2023), https://doi.org/10.1016/j.immuni.2023.01.029

STAR★METHODS

KEY RESOURCES TABLE

REAGENT or RESOURCE	SOURCE	IDENTIFIER
Antibodies		
VL4: Rat monoclonal anti-LCMV-NP	Dr. D.D. Pinschewer; Battegay et al.[88]	PMID: 1939506
Goat anti-rat IgG-HRP	Jackson Immunoresearch	Cat#112-035-003; RRID: AB_2338128
Anti-mouse TCF-1 (C63D8)	Cell Signaling	Cat# 2203T
Donkey anti-rabbit IgG (Poly4064) BV421	BioLegend	Cat# 406410, RRID:AB_10897810
Donkey anti-rabbit IgG PE	Biolegend	Cat#406421 RRID:AB_ 2563484
Anti-mouse/ CD8 (53-6.7) APC-Cy7	BioLegend	Cat# 100713 RRID:AB_312752
Anti-mouse CD4 (RM4.5) R718	BD Bioscience	Cat# 566940, RRID: AB_ 2869957
Anti-mouse CD45R/B220 (RA3-6B2) A700	Invitrogen	Cat#56-0452-82 RRID: AB_891458
Anti-mouse CD45R/B220 (RA3-6B2) PE	BD Biosciences	Cat#553089 RRID: AB_394619
Anti-mouse CD45.1 (A20) BV421	BioLegend	Cat#110731 RRID:AB_10896425
Anti-mouse CD45.1 (A20) FITC	BioLegend	Cat#110705 RRID: AB_313494
Anti-mouse CD45.2 (104) APC	BioLegend	Cat#109813 RRID: AB_389210
Anti-mouse CD45.2 (104) FITC	BioLegend	Cat#109805 RRID: AB_313442
Anti-mouse CD45.2 (104) BV785	BioLegend	Cat#109839 RRID:AB_2562604
Anti-mouse CD45.2 (104) PerCP/Cyanine 5.5	BioLegend	Cat# 109828 RRID: B_893350
Anti-mouse Ter-119 (ter119) BV650	BioLegend	Cat#116235 RRID:AB_11204244
Anti-mouse GP38/Podoplanin (8.1.1) PE	BioLegend	Cat#144606 RRID: AB_2562185
Anti-mouse CD31 (CD31) PE-Cy7	Biolegend	Cat#102418 RRID: AB_830757
Anti-mouse Ly108 (330-AJ) APC	BioLegend	Cat#134609 RRID:AB_2728154
Anti-mouse CD62L (MEL-14) PE-Cy7	BioLegend	Cat# 104418, RRID:AB_313103
Anti-mouse CX3CR1 (RUO) BV711	Biolegend	Cat#149031 RRID:AB_2565939
Anti-mouse PD-1 (29F.1A12) BV605	BioLegend	Cat#135219 RRID:AB_11125371
Anti-mouse Tim-3 (5D12) BV421	BD Biosciences	Cat#566346 RRID:AB_2739702
Anti-mouse CD69 (H1.2F3) PE	BioLegend	Cat# 104508, RRID: AB_313111
Anti-mouse Tbet (4B10) PE	eBioscience	Cat#12-5825-82 RRID: AB_925761
Anti-mouse/human Tox (TXRX10) PE	eBioscience	Cat#12-6502-82 RRID:AB_10855034
Anti-mouse Eomes (Dan11mag) PE	eBioscience	Cat# 12-4875-82 RRID: AB_1603275
Anti-mouse IFNg (XMG1.2) APC	Biolegend	Cat# 505810, RRID: AB_315404

(*Continued on next page*)

Please cite this article in press as: Marx et al., The alarmin interleukin-33 promotes the expansion and preserves the stemness of Tcf-1^{+} CD8^{+} T cells in chronic viral infection, Immunity (2023), https://doi.org/10.1016/j.immuni.2023.01.029

Continued

REAGENT or RESOURCE	SOURCE	IDENTIFIER
Anti-mouse/human Granzyme B (GB11) A647	Biolegend	Cat# 515406 RRID:AB_2566333
Anti-mouse Ki67 (SolA15), PerCP-eFluor 710	eBioscience	Cat#46-5698-82 RRID:AB_11040981
Mouse IgG1 kappa Isotype Control (P3.6.2.8.1), PE	eBioscience	Cat#12-4714-81 RRID: AB_ 470059
Polyclonal rat IgG	BioXcell	Cat#BE0094 RRID: AB_1107795
Anti-mouse CD8 (53-6.7) PerCP-Cyanine 5.5	eBioscience	Cat#45-0081-82 RRID: AB_1107004
Anti-mouse CD8 (53-6.7) Biotin	eBioscience	Cat#13-0081-82 RRID: AB_466346
Anti-mouse CD44 (IM7) APC-Cy7	Biolegend	Cat#103028 RRID: AB_830785
Streptavidin PE	BD Biosciences	Cat# 554061 RRID: AB_10053328
Anti-Mouse CXCR3 (CXCR3-173) BV421	Biolegend	Cat# 126529 RRID:AB_2563100
Goat anti-Rabbit IgG (H+L) A647	eBioscience	Cat# A-21244 RRID:AB_2535812
ImPRESS HRP Goat Anti-Rat IgG	Vector Laboratories	Cat#MP-7444-15; RRID: AB_2336530
Antibodies for histology		
Rat, Anti-mouse B220 (RA3-6B2)	Dr. Sanjiv Luther	N/A
Rabbit, Anti-mouse IFNα (PAb)	PBL assay science	Cat#PBL-32100
Goat, Anti-mouse IL-33	R&D	Cat#AF3626
Goat, anti-mouse GFP (polyclonal)	Abcam	Cat#AB6673
Chicken, anti GFP (PAb)	Abcam	Cat#Ab13970
Rabbit, anti-mouse GFP (PAb)	Invitrogen	Cat#A11122 RRID: AB_221569
Mouse anti-mouse CD45.1 biotinylated (A20.1)	Dr. Sanjiv Luther	N/A
Donkey-anti goat Alexa647	Thermo Fisher	Cat#A-21447 RRID :AB_2535864
Cy3 AffiniPure Donkey Anti-Rabbit IgG (H+L)	Jackson Immunoresearch	Cat#711-165-152 RRID : AB_2307443
Cy3 AffiniPure Donkex Anti-Goat IgG (H+L)	Jackson Immunoresearch	Cat#705-165-147 RRID : AB_2307351
Donkey anti-rat Alexa488	Invitrogen	Cat#A21208 RRID :AB_2535794
AffiniPure Donkey Anti-Chicken IgY (IgG) (H+L), Alexa Fluor488	Jackson Immunoresearch	Cat#703-545-155 RRID :AB_2340375
Streptavidin-BV421	Biolegend	Cat#405226
Anti-Mouse IL-4 (11B11)	Dr. Max Löhning	N/A
Bacterial and Virus Strains		
LCMV Cl13	Ahmed et al.[89]	N/A
artLCMV	Dr. D.D. Pinschewer; Kallert et al.[41]	N/A
rAd-GP vector	Dr. D.D. Pinschewer This paper.	N/A
Chemicals, Peptides, and Recombinant Proteins		
Brefeldin A	Invitrogen	Cat#B7450
DAB	DAKO	Cat#K5001
Heparin Na 25000 I.E./5 ml	B. Braun Medical	Cat#B01AB01
TRI reagent LS	Sigma-Aldrich	Cat#T3934-100ML

(*Continued on next page*)

Please cite this article in press as: Marx et al., The alarmin interleukin-33 promotes the expansion and preserves the stemness of Tcf-1^{+} CD8^{+} T cells in chronic viral infection, Immunity (2023), https://doi.org/10.1016/j.immuni.2023.01.029

Continued

REAGENT or RESOURCE	SOURCE	IDENTIFIER
LCMV GP33-41 KAVYNFATC	GenScript Biotech	N/A
H-2D(b) LCMV GP 33-41 KAVYNFATC – APC-labeled	NIH Tetramer Core Facility at Emory University University of Lausanne Tetramer core facility	N/A
Mouse IL-2	Miltenyi Biotec	Cat#130-098-221
Mouse IL-7	Miltenyi Biotec	Cat#130-094-066
Mouse IL-12	Miltenyi Biotec	Cat#130-096-795
Mouse IL-33	R&D	Cat#3626-ML-010
Brefeldin A	Sigma-Aldrich	Cat#B6542
ß-Mercaptoethanol	Sigma-Aldrich	Cat#7522
Histopaque-1083	Sigma-Aldrich	Cat#10831
Critical Commercial Assays		
BD FACS Lysing solution	Becton, Dickinson and Company BD Bioscience	Cat#349202
e Bioscience 7-AAD Viability Staining Solution	Biolegend	Cat#420404
EdU-Imaging kit EdU-Click 488, baseclick	Baseclick	Cat#BCK488-IV-FC-L
eBisoscience FoxP3/Transcription Factor Staining Buffer Set	eBiosicences	Cat#00-5523-00
Miltenyi Biotec naïve CD8 T cell isolation kit, mouse	Miltenyi, Biotec	Cat# 130-096-543
Miltenyi Biotec, FASER-kit-PE	Miltenyi Biotec	Cat#130-091-764
Miltenyi Biotec, Anti-Biotin Micro Beads	Miltenyi Biotec	Cat#130-090-485
Zombie UV fixable viability kit	BioLegend	Cat#423108
Bioanalyzer High Sensitivity RNA Analysis, Agilent RNA 6000 Pico Kit	Agilent	Cat#5067-1513
QuantiFluor RNA System	Promega, Madison, WI, USA	Cat#E3310
TruSeq Stranded mRNA Libary Kit	Illumina, San Diego, CA, USA	Cat#20020595
TruSeq RNA UD Indexes	Illumina, San Diego, CA, USA	Cat#20022371
NGS Fragment Analysis Kit	Advanced Analytical	Cat#DNF-473
NextSeq 500 High Output Kit 75-cycles	Illumina, San Diego, CA, USA	Cat#FC-404-1005
QantiFluor ONE dsDNA Sytem	Promega, Madison, WI, USA	Cat#E4871
Direct-zol™ RNA MicroPrep kit	Zymo research	Cat#R2060
CellTrace™ Violet Cell Proliferation Kit	Invitrogen	Cat#C34557
NucleoSpin RNA XS Micro Kit	Macherey & Nagel	Cat# 740902.250
Taqman reverse transcription reagents	Applied Biosystems	Cat#N8080234
TaqMan Fast Advanced Master Mix	Applied Biosystems	Cat# 4444556
Taqman Gene expression assay *Tcf7*, Mm00493445_m1	Thermo Scientific	Cat# 4331182
Taqman Gene expression assay *Hprt*, Mm00446968_m1	Thermo Scientific	Cat# 4351370
DNA Clean and Concentrator ™5	Zymo Research	Cat# D4013
AMPure XP Reagent, 450	Beckman Coulter	Cat# A63882
Deposited Data		
Raw and Analyzed Data	This Paper	Zenodo: 6759144
RNA-seq data	This Paper	GEO:GSE210538 GEO:GSE210537
ATAC-seq data	This Paper	GEO:GSE210536

(*Continued on next page*)

Please cite this article in press as: Marx et al., The alarmin interleukin-33 promotes the expansion and preserves the stemness of Tcf-1^{+} CD8^{+} T cells in chronic viral infection, Immunity (2023), https://doi.org/10.1016/j.immuni.2023.01.029

Continued

REAGENT or RESOURCE	SOURCE	IDENTIFIER
Experimental Models: Cell Lines		
Mouse: NIH 3T3	ATCC	Cat#CRL-1658 RRID::CVCL_0594
Hamster: BHK-21	ECACC	Cat#85011433 RRID: CVCL_1915
Experimental Models: Organisms/Strains		
Mus musculus: (ST2-deficient (ST2$^{-/-}$) *Il1rl1*$^{-/-}$) B6.129S-Il1rl1<tm1>/McK	Bonilla et al.[37]; Townsend et al.[90]	N/A
Mus musculus: C57BL/6J	Charles River	JAX: 000664
Mus musculus: (*Il33*$^{gfp/gfp}$ mice, also referred to as *Il33*$^{-/-}$) Il33tm1Snak (MGI: 4838250)	Oboki et al.[91], obtained through the RIKEN Center for Developmental Biology-Acc. No: CDB0631K	N/A
Mus musculus: (*Ifnar1*$^{-/-}$) B6.129Sv/Ev-IFNaRtmAgt	Muller et al.[92]	N/A
Mus musculus: (*Tcf7*^{gfp} mice) B6.Tg(Tcf7^{GFP}) Whe (Tcf7^{GFP}) (CD45.2)	Utzschneider et al.[12]	N/A
Mus musculus: (LCMV GP33-specific TCR-transgenic P14 TCR mice) B6-Tg(TCRP14)327	Pircher et al.[51]	N/A
Mus musculus: (*Ccl19*Cre^{+}) B6 Tg(BAC-CCL19Cre)	Chai et al.[93]	N/A
Mus musculus: (*Ifnar1*$^{fl/fl}$) Ifnar1tm1Uka	Prinz et al.[94]	N/A
Mus musculus: (*Il33*$^{fl/fl}$) B6-Il33<tm1.1Rlee	Chen et al.[95]	N/A
Mus musculus: B6.129P2-*Tcrb*^{tm1Mom} *Tcrd*^{tm1Mom}/J (*TCRβδ*$^{-/-}$)	Jackson Laboratory	JAX:002122
Software and Algorithms		
Prism 9.0.0	GraphPad Software	RRID: SCR_002798
FlowJo 10.5.3	Becton Dickinson & Company	RRID: SCR_008520
Adobe Illustrator CC 2022	Adobe Photoshop	RRID:SCR_010279
STAR 2.7.0c	Dobin et al., 2013[96]	N/A
bowtie2 2.4.2	Langmead and Salzberg, 2012[97]	N/A
macs2 2.1.2.1	Zhang et al., 2008[98]	N/A
samtools 1.11	Li et al.[99]	N/A
R 4.1.3	R Core Team	https://www.R-project.org/.
Bioconductor 3.14	Huber et al.[100]	N/A
Visiopharm with TissueAlign Module 2021.09	Visiopharm	N/A
QuantStudio Real-Time PCR Software v1.2	Applied Biosystems	N/A
clusterProfiler (v4.4.3)	Bioconductor	https://bioconductor.org/packages/release/bioc/html/clusterProfiler.html
DESeq2 (v1.36.0)	N/A	https://bioconductor.org/packages/release/bioc/html/DESeq2.html
ARCHS4	N/A	https://maayanlab.cloud/archs4/
Seurat (v4.0.1)	N/A	https://github.com/satijalab/seurat
sctransform (v0.3.3)	N/A	https://github.com/satijalab/sctransform
edgeR (v3.40.0)	N/A	https://bioconductor.org/packages/release/bioc/html/edgeR.html
ComplexHeatmap (v2.14.0)	N/A	https://www.bioconductor.org/packages/release/bioc/html/ComplexHeatmap.html
hallmark gene sets MSigDB (version 7.0)	N/A	http://www.gsea-msigdb.org/gsea/index.jsp
Devices/Other		
QuantStudio 7 Flex Real-Time PCR System	Applied Biosystems	N/A
BD FACS Canto II	BD Biosciences	N/A
MACS Quant Analyzer 10	Miltenyi Biotec	N/A

(*Continued on next page*)

Please cite this article in press as: Marx et al., The alarmin interleukin-33 promotes the expansion and preserves the stemness of Tcf-1^{+} CD8^{+} T cells in chronic viral infection, Immunity (2023), https://doi.org/10.1016/j.immuni.2023.01.029

Continued

REAGENT or RESOURCE	SOURCE	IDENTIFIER
BD FACS Canto II	BD Biosciences	N/A
BD LSRFortessa	BD Biosciences	N/A
5-laser Aurora spectral flow cytometer	Cytek Bioscience, Fremnont, CA,USA	N/A

RESOURCE AVAILABILITY

Lead contact

Further information and requests for resources and reagents should be directed to and will be fulfilled by the lead contact, Daniel Pinschewer (daniel.pinschewer@unibas.ch).

Materials availability

Material transfer agreements with standard academic terms will be established to document reagent sharing by the lead contact's institution. ST2$^{-/-}$ mice[37,90] will be made available upon establishment of an MTA between the recipient and MRC Cambridge, UK.

Data and code availability

- Raw data of the experimental results reported in this study have been deposited with Zenodo and are publicly available as of the date of publication under the DOI https://doi.org/10.5281/zenodo.6759144.
- RNAseq and ATACseq data are deposited with the National Center for Biotechnology Information Gene Expression Omnibus (GEO) under the accession numbers GSE210536, GSE210537, GSE210538 respectively.
- Any additional information required to reanalyze the data reported in this paper is available from the lead contact upon request.

EXPERIMENTAL MODEL AND SUBJECT DETAILS

Animals and ethics statement

ST2-deficient *Il1rl1*$^{-/-}$,[37,90] *Il33*$^{gfp/gfp}$ mice[91] (also referred to as *Il33*$^{-/-}$, obtained through the RIKEN Center for Developmental Biology-Acc. No: CDB0631K), *Ifnar1*$^{-/-}$,[92] *Tcf7*^{gfp} mice,[12] LCMV GP33-specific TCR-transgenic P14 TCR mice,[51] *Ccl19*Cre^{+}[93] (generously provided by Dr. Burkhard Ludewig), *Ifnar1*$^{fl/fl}$[94] (generously provided by Dr. Ulrich Kalinke) and *Il33*$^{fl/fl}$ [95] mice have been described. TCR$\beta\delta^{-/-}$ (B6.129P2-*Tcrb*^{tm1Mom} *Tcrd*^{tm1Mom}/J; Jackson: JAX:002122) have been obtained from Jackson Laboratory. P14 *Il1rl1*$^{-/-}$, P14 *Ifnar1*$^{-/-}$, *Ccl19*-Cre$^{-/+}$ *Ifnar1*$^{fl/fl}$ and Ccl19-Cre$^{-/+}$ *Il33*$^{fl/fl}$ mice were obtained by intercrossing with the respective parental lines. C57BL/6J (WT) mice were bred at the at the Laboratory Animal Science Center (LACS) of the University of Zürich and at the ETH Phenomics Center (EPIC). All animals were on a C57BL/6J background as verified by single nucleotide polymorphism (SNP) typing (Taconic Biosciences). Mouse experiments were performed at the University of Basel with authorization from the respective Cantonal veterinary offices and at the German Rheumatism Research Center (DRFZ) in Berlin, Germany, with approval from the State Office for Health and Social Services (Landesamt für Gesundheit und Soziales), Berlin, Germany. All experiments were carried out in accordance with the Swiss law for animal protection and the European directive 155 2010/63/EU on Care, Welfare and Treatment of Animals, respectively, and mice were kept under specific-pathogen-free (SPF) conditions at all locations. Animals in experimental groups were sex- and age-matched. Animals of both genders were used to reduce the number of animals bred for research purposes. Sample sizes in the studies were chosen based on long-standing experience in our labs with respect to group sizes generally revealing biologically significant differences. The groups were not randomized and the experiments were not conducted in a blinded fashion. Animals were bred at the Laboratory Animal Science Center (LACS) of the University of Zürich, at the ETH Phenomics Center (EPIC) and at the Research Institute for Experimental Medicine (FEM) of the Charité – Universitätsmedizin Berlin, Berlin, Germany.

METHOD DETAILS

Viruses, virus titrations, infections and immunizations

LCMV strain clone 13[89] was produced by infecting BHK-21 cells at a multiplicity of infection (MOI) of 0.01. The supernatant was harvested 48h later and viral titers were determined by focus forming assay on 3T3 cells as described.[37,88] Mice were infected with $\geq 2x10^6$ plaque forming units (PFU) of LCMV intravenously (i.v.). artLCMV has been described[41] and was administered at a dose of $1x10^6$ PFU i.v. The rAd-GP vector used in this study is an Ad5-based E1-deleted first generation vector, which was generated by transfecting the corresponding infectious plasmids into the E1-transcomplementing 293 cell line. It expresses the LCMV glycoprotein (full length) and a green fluorescent protein (GFP) under the cytomegalovirus (CMV) promotor, replacing the E1 gene of Ad5. The vector was purified by double discontinuous CsCl density gradient centrifugation and the physical titer was determined by OD260. It was administered to mice at a dose of $5x10^8$ genome copies i.v.. To measure LCMV viremia of mice, ~50 µl of whole blood was collected into 950 µl of BSS supplemented with heparin (Na-heparin, Braun, 1 IE/ml final).

Please cite this article in press as: Marx et al., The alarmin interleukin-33 promotes the expansion and preserves the stemness of Tcf-1$^+$ CD8$^+$ T cells in chronic viral infection, Immunity (2023), https://doi.org/10.1016/j.immuni.2023.01.029

Staining of cells for flow cytometric analysis

To study T cells, single-cell suspensions of spleens were prepared by mechanical disruption using a metal mesh. Surface staining was performed at 4°C in the dark for 30 mins. All stains were performed in FACS buffer (PBS supplemented with 2% FCS, 5mM EDTA, 0.05% sodium azide).

For the detection of GP33-specific CD8$^+$ T cells, MHC class I tetramers (H-2D^b) loaded with the immunodominant LCMV glycoprotein- (GP-) derived GP$_{33-41}$ peptide (KAVYNFATC) were obtained from the NIH Tetramer Core Facility and from the University of Lausanne Tetramer core facility. Cells exhibiting non-specific binding were excluded by pre-gating on B220$^-$CD4$^-$CD8$^+$ cells. Tetramer staining was performed at RT for 30 mins in the dark.

Antibodies against CD8$^+$ (53-6.7), CD4 (IM7 or RM4-5), B220 (RA3-6B2), CD45.1 (A20), CD45.2 (104), Ter-119 (TER-119; dilution: 1:10), GP38-Podoplanin (8.1.1; dilution: 1:250), CD31 (390), Ly108 (330-AJ), CD62L (MEL-14), CX3CR1 (SA01F11), PD-1 (29F.1A12) and Tim-3 (5D12), CD69 (H12F3) were obtained from Biolegend, eBioscience/ThermoFisher or BDBioscience/PharMingen. Unless indicated differently, all fluorescently labelled monoclonal antibodies were used at a 1:100 final dilution.

Dead cells were excluded using either 7-AAD or the Zombie UV Fixable Viability Kit (Biolegend) according to manufacturer's instructions.

When staining cells in peripheral blood, samples were fixed and lysed by adding 1 ml/sample of eBioscience 1-step Fix/Lyse Solution and incubating at RT for 5min. The reaction was stopped by adding FACS-buffer.

To evaluate in cells the expression levels of transcription factors we used antibodies to Eomes (Dan11mag), T-bet (4B10) and Tox (TXRX10), which we used according to the protocol included in the eBioscience™ FOXP3 transcription factor staining kit (Invitrogen). Isotype control antibodies were used for Eomes (eBR2a, eBioscience/ThermoFisher) and Tbet (P3.6.2.8.1, eBioscience/ThermoFisher). Ki67 (SolA15, Invitrogen, 1:1000 dilution) staining was performed with the eBioscience™ FOXP3 transcription factor staining kit (Invitrogen).

The transcription factor Tcf-1 was detected by incubating first with a primary antibody (C63D8, Cell Signaling, at 1: 200 dilution) followed by donkey anti-rabbit IgG PE (Poly4064-eBioscience). For the detection of ST2, which on type-1 immune cells such as CD8$^+$ T cells and Th1 cells is expressed in substantially lower amounts than on type-2 immune cells[87] spleen cells were stained with digoxigenin-coupled anti-mouse ST2 antibody (DJ8). As a secondary antibody, a PE-coupled anti-digoxigenin Fab (Roche) antibody was used. To further amplify the signal, two rounds of signal amplification were performed using the PE-FASER Kit (Miltenyi Biotec).

To analyze fibroblastic reticular cells (FRCs), spleens were cut into small pieces and incubated in RPMI (2% vol/vol FCS; containing 1mg/ml Collagenase IV (Worthington) and 40 μg/ml DNAseI (Roche) for 30 minutes at 37°C, stirring at a speed of 250 rpm. To stop the enzymatic reaction, FACS buffer was added. Erythrocytes were lysed by adding 1ml/spleen of ACK lysis buffer (0.15 M NH_4Cl, 10mK $KHCO_3$, 0.1 mM EDTA) and the reaction, conducted at room temperature (RT), was stopped after 60 seconds by adding FACS buffer. Hematopoietic CD45$^+$ cells were depleted by using anti-CD45 beads (Miltenyi Biotec) following the manufacturer's instructions. For analysis of FRCs, erythrocytes (Terr119$^+$) and hematopoietic cells (CD45$^+$) were excluded. To distinguish FRC from blood endothelial cells (BEC) we relied on the endothelial marker CD31 and the fibroblastic marker gp38 (podoplanin) as shown in Figure S3M.

For intracellular cytokine staining of CD8$^+$ T cells, splenocytes were stimulated with 1μg/ml of MHC class I restricted LCMV-GP$_{33-41}$ for 1h at 37°C in a 5% CO_2 incubator. After 1 hour incubation, Brefeldin A (final concentration: 10 μg/ml) was added to the cells followed by additional 4 hours of incubation. Surface staining was performed as above. Afterwards, cells were fixed with 2% PFA for 10 min followed by permeabilization with staining buffer supplemented with 0.05% saponin (Sigma-Merck, Germany). Intracellular staining was performed with antibodies to IFN-γ (XMG1.2, Biolegend) and Granzyme B (GB11, Biolegend).

Samples were measured on a BD LSRFortessa flow cytometer and on a 5-laser Aurora spectral flow cytometer (Cytek Biosciences, Fremnont, CA, USA). FlowJo Software (Becton Dickinson) was used for analysis.

Cell transfer followed by next-generation RNA sequencing or ATAC sequencing and bioinformatic data analyses

To assess the impact of IL-33 signals on the CD8$^+$ T cell transcriptome on day 6 after LCMV infection we co-transferred 10^3 MACS-purified (Miltenyi Biotec naïve CD8$^+$ T cell isolation kit, mouse) P14 WT and 3x10^3 MACS-purified P14 *Il1rl1*$^{-/-}$ cells into WT recipients in a set-up analogous to Figure 1J. P14 progeny cells after LCMV infection were FACS-sorted and processed for RNAseq. This experimental set-up allowed us to recover equal number of both P14 cell subsets on day 6 after infection.

For the assessment of the transcriptome accessibility of P14 WT *Tcf7*^{gfp} cells and of P14 *Il1rl1*$^{-/-}$ *Tcf7*^{gfp} cells on day 4 after LCMV infection, we single transferred 10^6 MACS-purified cells of either type (Miltenyi Biotec naïve CD8$^+$ T cell isolation kit, mouse) into WT recipients. *Tcf7*$^{gfp+}$ and *Tcf7*$^{gfp-}$ were FACS-sorted on day 4 after LCMV infection and were processed for RNAseq.

In either set-up, cells were sorted on a FACSAria II (BectonDickinson), collected directly into Trizol LS (Sigma-Aldrich) and stored at -80°C until RNA extraction. RNA was extracted using the Direct-zol™ RNA MicroPrep kit (Zymo research).

RNA quality from samples sorted on day 6 after infection (Figures 1J–1M) was checked on the Bioanalyzer instrument (Agilent Technologies, Santa Clara, CA, USA) using the RNA 6000 Pico Chip (Agilent, Cat# 5067-1513). Average RIN (RNA Integrity Number) was quantified by Fluorometry using the QuantiFluor RNA System (Cat# E3310, Promega, Madison, WI, USA). Library preparation was performed, starting from 35 ng total RNA, using the TruSeq Stranded mRNA Library Kit (Cat# 20020595, Illumina, San Diego, CA, USA) and the TruSeq RNA UD Indexes (Cat# 20022371, Illumina, San Diego, CA, USA). 15 cycles of PCR were performed. Libraries were quality-checked on the Fragment Analyzer (Advanced Analytical, Ames, IA, USA) using the Standard Sensitivity NGS Fragment Analysis Kit (Cat# DNF-473, Advanced Analytical) revealing excellent quality of libraries (average concentration was 63±12 nmol/L and average library size was 317±4 base pairs). Samples were pooled to equal molarity. The pool was quantified

by Fluorometry using the QuantiFluor ONE dsDNA System (Cat# E4871, Promega, Madison, WI, USA). Libraries were sequenced Single-reads 76 bases (in addition: 8 bases for index 1 and 8 bases for index 2) using the NextSeq 500 High Output Kit 75-cycles (Illumina, Cat# FC-404-1005) loaded at 2.0pM, and including 1% PhiX.Primary data analysis was performed with the Illumina RTA version 2.11.13. The NextSeq run yielded on average per sample 19.7±1.6 millions pass-filter reads.

RNA from samples sorted on day 4 after infection (Figure 5A) were quality-checked on the Bioanalyzer instrument (Agilent Technologies, Santa Clara, CA, USA) using the RNA 6000 Pico Chip (Agilent, Cat# 5067-1513) and quantified by Fluorometry using the QuantiFluor RNA System (Cat# E3310, Promega, Madison, WI, USA). Library preparation was performed, starting from 4.5ng total RNA, using the SMART-Seq v4 PLUS Kit (Cat# R400753, Takara Bio). Libraries were quality-checked on the Fragment Analyzer (Advanced Analytical, Ames, IA, USA) using the Standard Sensitivity NGS Fragment Analysis Kit (Cat# DNF-473, Advanced Analytical) revealing excellent quality of libraries (average concentration was 31±5 nmol/L and average library size was 508±27 base pairs). Samples were pooled to equal molarity. The pool was quantified by Fluorometry using the QuantiFluor ONE dsDNA System (Cat# E4871, Promega, Madison, WI, USA). Libraries were sequenced Paired-End 51 bases (in addition: 8 bases for index 1 and 8 bases for index 2) using the NovaSeq 6000 instrument (Illumina) and the SP Flow-Cell loaded at a final concentration in Flow-Lane of 400pM and including 1% PhiX. Primary data analysis was performed with the Illumina RTA version 3.4.4. On average per sample: 32.2±2.8 millions pass-filter reads were collected on 1 SP Flow-Cell.

Reads were aligned to the mouse genome (UCSC version mm10) with STAR version 2.7.0c[96] with additional settings '--outFilterMultimapNmax 10 –outSAMmultNmax 1' to account for multi-mapping reads. Mapped reads were assigned to genes based on the Ensembl 96 gene annotation using the function featureCounts (Subread package, version 1.6.4) and either extra options '-O –read2pos 5 –M –s 2' for the TruSeq, single-end sequencing libraries generated from day 6 data or '-O –read2pos 5 –M –s 0 -p -B' for the SmartSeq, paired-end libraries of day4 data.

For mRNAseq analysis on day 4 (Figure 5), differential expression analysis used functions of the edgeR package.[101] First genes were filtered using the filterByExpr function with default settings (n= 29238 genes). In the following, two different designs were analyzed: for the comparison of *Il1rl1*$^{-/-}$ vs. WT within the Tcf$^+$ and Tcf- populations respectively a simple model accounting for all four sample groups was fit using the glmQLFit function and the comparison under study was tested using the function glmQLFTest and topTags with default settings. Significantly regulated genes were defined having an FDR adjusted p. value < 0.05 and an absolute $\log_2$FC > 1.5. A second, more complex model was used for the comparison of Tcf$^+$ vs. Tcf- samples within a given genotype and also accounted for the replicate effect. The comparison under study was tested using the same edgeR functions mentioned above. PCA analysis relied on log-CPM transformed expression values and used the function prcomp.

For mRNAseq analysis day 6 data (Figure 1), only genes with biotypes "protein coding", "long non-coding" or "short non-coding" where considered in the analysis. Additionally, only genes with a logCPM>1 in at least 5 samples were retained resulting in n=11032 detected genes. Differential gene expression analysis between the genotypes relied on functions from the R/Bioconductor package edgeR as detailed above (R version 4.1.1, Bioconductor version 3.14.0).[100] Differential regulation of all hallmark gene sets from MSigDB (version 7.0) was evaluated using the function 'camera' from edgeR with extra options 'inter.gene.cor = 0.01'. The average absolute log fold change of a gene set was used as a proxy for its strength of regulation. The ComplexHeatmap package was used to draw heatmaps.[102]

For ATAC-seq analysis of P14 WT *Tcf7*$^{gfp+}$ cells and of P14 *Il1rl1*$^{-/-}$ *Tcf7*$^{gfp+}$ cells on day 4 after LCMV infection (Figures 5B–5E), we individually transferred 10^6 MACS-purified cells of either genotype (Miltenyi Biotec naïve CD8$^+$ T cell isolation kit, mouse) into WT recipients. 20 000 *Tcf7*$^{gfp+}$ were FACS-sorted on day 4 after LCMV infection into 500 μl of lymphocytic medium and were processed for ATAC-seq. Library preparation for sequencing was performed as described.[103] Briefly, sorted cells were lysed and tagmentated for 30 min at 37°C using the Illumina Tagment DNA Enzyme and Buffer Kit. DNA was purified with the Zymo DNA Clean and Concentrator Kit and amplified for five cycles using the NEBNext® High-Fidelity 2x PCR Master Mix and Custom Nextera Index Primers (Illumina). The number of additional cycles was determined by Real-time PCR as the number of cycles needed to reach ¼ of maximum fluorescent intensity. After the second amplification step, DNA was cleaned up using AMpure XP beads and sequenced on an Illumina NexSeq 50 machine using 41-bp paired-end run. Paired-end reads were aligned to the UCSC mm10 genome using bowtie2 version 2.4.2[97] with additional parameter settings "-maxins 2000 -no-mixed -no-discordant -local" and resulting BAM files were sorted and indexed with samtools version 1.11.[99] For each group of biological replicates, regions of accessible chromatin were called with macs2 version 2.1.2.1[98] using the option '-f BAM -g 2652783500 –nomodel –shift -100 –extsize 200 –broad –keep-dup all –qvalue 0.05'. All further analysis was performed in R. The resulting peak lists were cleaned from peaks called in mitochondria, chrX and chrY, and ENCODE blacklist regions. Additionally, we applied a log-fold-change > 1.5 and FDR adjusted p. value < 0.05 filter. In the next step, genotype-specific peak lists were combined into one list where peaks regions in a distance less than 250 based were merged. This resulted in a list of 209664 peaks. Next, 5'-ends overlapping with these peaks were counted using function bamCount of the bamsignals R package to obtain the count matrix used for differential accessibility analysis. Differential accessibility analysis was performed using functions from the edgeR R package. First, the count matrix was further filtered for peaks that had a log-RPKM value bigger than 1 in at least 4 samples. This resulted in 59964 peaks to be tested for differential accessibility. Next, functions estimateDisp, glmQLFit, and glmQLFTest were used to test the ST2$^{-/-}$ versus WT contrast. To detect genotype-specific peaks we filtered for peaks with an FDR adjusted p. value < 0.05 and logFC > 1.5 (=ST2$^{-/-}$ specific; 17 peaks) or logFC < -1.5 (=WT specific; 566 peaks). 59964 peaks were in common by that definition. Function detailRanges of the csaw package[104] was used to annotate peaks. Read coverage tracks of genomic loci under study were plotted using the GViz R package.[105]

Please cite this article in press as: Marx et al., The alarmin interleukin-33 promotes the expansion and preserves the stemness of Tcf-1$^+$ CD8$^+$ T cells in chronic viral infection, Immunity (2023), https://doi.org/10.1016/j.immuni.2023.01.029

To test for differential transcription factor (TF) binding site occurrences in the sets of genotypes, specific versus common peaks, we predicted TF binding sites in all peaks used for differential accessibility analysis. Specifically, we focused on all vertebrate TFs as given by the JASPAR2018 R package (n = 579). For these we use the matchMotifs function of the motifmatchr R package to predict binding sites using a p-value cutoff of 5e-5. For each TF motif we tested the overrepresentation of sites in either *Il1rl1*$^{-/-}$ specific or WT-specific peaks relative to the common peaks using the fisher.test R function with option alternative="greater". P-values were FDR corrected across TF motifs but separately for *Il1rl1*$^{-/-}$ and WT specific tests. Using the FDR adjusted p. Value < 0.05 threshold resulted in 38 TF motifs that were enriched in WT-specific versus common peaks. Based on their predicted binding site overlap these 38 TF motifs can be grouped into 4 TF motif classes as shown in Figure 5.

Identification of ATAC peaks specific for stem-like, memory and exhausted CD8$^+$ T cells

For generation of coverage tracks and calling of peaks with MACS2, the data of Jadhav et al.[24] was processed in the same way as outlined in the above paragraph. Peaks were additionally filtered for a q-value < 0.01 and a logFC > 2.5. We defined the following two peak lists for each of the two cell-types to characterize (stem-like, memory):

1. peaks common to the cell type and to exhausted T cells (“common peaks”)
2. cell type-specific peaks by contrast to exhausted T cells (“cell type-specific peaks”))

To count the overlap of our WT specific peak list with those defined above we use the findOverlaps function of the R/Bioconductor package GenomicRanges with default settings. The significance of the overlap was quantified with function fisher.test in R which used as an input a contingency table with the following peak overlap counts:

1. Number of overlapping WT-specific and cell type-specific peaks
2. Number of WT-specific peaks not overlapping with cell type-specific peaks
3. Number of WT-specific peaks overlapping with common peaks
4. Number of WT-specific peaks not overlapping with common peaks.

Gene set enrichment analysis

Gene Set Enrichment analysis (GSEA)[106] was run with manually curated gene sets using the implementation of GSEA in the clusterProfiler 4.4.3[107] package in R with default settings. To manually curate gene sets from publicly available bulk RNA-seq data, gene counts from Gene Expression Omnibus Series accession codes GSE142687,[26] GSE83978[12] and GSE122713[52] were accessed using ARCHS4.[108] Next, canonical analysis of RNA-seq data was performed in R version 4.2.0 with DESeq2 version 1.36.0.[109] The gene set under study arbitrarily included the top 150 differentially expressed genes (DEGs) ranked by false discovery adjusted *P value* using the Benjamini-Hochberg correction. Publicly available single cell RNA-seq data from GSE131535 (GSM3785519)[21] and GSE119940 (GSM3568588 and GSM3568592)[53] were analyzed with the R package Seurat version 4.0.1.[110] Cells with more than 5000 or less than 1000 genes and cells with > 4% mitochondrial counts were excluded from downstream analysis to filter out probable cell doublets and cells of low quality. In addition, only genes detected in at least 10 cells were kept. Raw counts were normalized using the R package sctransform version 0.3.3[111] with the glmGamPoi method. Next, the three obtained datasets were integrated using the SelectIntegrationFeatures function of Seurat by identifying anchors between the three datasets on the top 3000 highly variable genes. Principal components analysis and Uniform Manifold Approximation and Projection (UMAP) dimensional reduction were performed using the first 30 principal components as input. Clustering using the FindNeighbors function of Seurat (with the first 30 principal components as input) and the FindClusters function (with a resolution of 0.4) identified one cluster with high expression of *Tcf7*. Positive and negatives marker genes of this cluster were identified with the FindMarkers function of Seurat run with default settings. The *Tcf7*$^+$ signature was curated by arbitrarily selecting the top 150 differentially expressed markers genes ranked by false discovery adjusted *P value* using the Bonferroni correction method.

For comparison of our P14 WT and P14 *Il1rl1*$^{-/-}$ mRNA-Seq data to those of P14 cells from IFNAR-blocked and control-treated mice[29] the mRNA-Seq data of Huang et al. was downloaded from GEO (GSE97139) and gene expression was quantified in the same way as our SmartSeq4 data set (mRNAseq analysis on day 4, reported in Figure 5A). Differential gene expression between α-IFNAR and isotype control samples was performed with edgeR as described above. The set of significantly regulated genes (FDR < 0.05 & abs(logFC) > 1.5) were filtered for genes expressed in our data set and were used as a gene set (n=107) for comparison. Gene set testing was done with function cameraPR of the edgeR package and relied on the F-test statistic to allow for a non-directional gene set test.

Adoptive T cell transfer for flow cytometric analysis and re-transfer

For adoptive cell transfer, P14 CD8$^+$ T cells (P14 cells) were MACS-purified (Miltenyi Biotec naïve CD8$^+$ T cell isolation kit, mouse) from the spleens of naïve donor mice and administered i.v. into the tail vein of recipients. For co-transfer of P14 WT and P14 *Il1rl1*$^{-/-}$ cells, equal numbers of both cell populations were mixed for i.v. injection. To ascertain clearly detectable populations of transferred cells, 10^4 cells were transferred for analysis on day 4 after LCMV, 10^3 cells for analysis on day 6. For analyses on day 9 and later, mice received 500 cells, thereby assuring P14 cells were in the physiological range of GP33-specific CD8$^+$ T cell precursor frequencies.[112] Transferred P14 cell populations were differentiated from the recipient’s CD8$^+$ T cells by means of their congenic

CD45.1 markers. When co-transferring P14 WT and P14 *Il1rl1*$^{-/-}$ cells, one population was CD45.1$^+$ single-positive the other one CD45.1$^+$CD45.2$^+$ double-positive.

For sequential adoptive transfer experiments, CD8$^+$ T cells were MACS-purified (Miltenyi Biotec naïve CD8$^+$ T cell isolation kit, mouse) from the spleens of naïve P14 *Tcf7*^{gfp} and P14 *Il1rl1*$^{-/-}$ *Tcf7*^{gfp} donor mice. 10^6 cells of either population were separately transferred into WT primary recipient mice followed by LCMV infection. Four days later, the progeny of transferred P14 cells were sorted on FACSAria II (BectonDickinson) into RPMI supplemented with 10 % FCS and 1% penicillin/streptomycin. Equal numbers of each cell type (~1x10^3 -1x10^4) were re-transferred into WT secondary recipient mice. Secondary recipients were infected with either LCMV (on the day of re-transfer) or with rAd-GP two weeks after re-transfer.

In vivo blockade of type I interferon receptor, *in vivo* blockade of IFN-γ and NK cell depletion

To block the interferon type I receptor (IFNAR), mice were given 1 mg of α-IFNAR monoclonal antibody (MAR-1-5A3, BioXcell) one day prior to infection. Control groups were administered 1 mg of isotype control antibody (MOPC-21, BioXcell). To block IFN-γ, mice were given a single dose of 2 mg of the monoclonal rat antibody XMG1.2 (anti-IFN-γ, Bioxcell) one day prior to infection. Control groups were left untreated. For transfer experiments involving P14 *Ifnar1*$^{-/-}$ cells, NK cells were depleted as described in. [59] In brief, 300 μg of α-NK.1.1 (clone PK136, BioXcell) monoclonal antibody was administered to mice on day -1 and on day 1 of LCMV infection.

Generation of bone marrow chimeric mice

Recipients of bone marrow (irradiated mice received 7.5x10^6 cells of WT and Il1rl1$^{-/-}$ BM cells) were lethally irradiated (1.1 Gy; twice 5.5 gray at a 6-hour interval) the day before transfer, and residual T cells were depleted by intraperitoneally administering 100 μg anti-Thy1 antibody (clone T24, BioXcell). The animals were rested for 7 weeks before infection.

Proliferation analysis

To assess the impact of IL-33 signals on the proliferative activity of CD8$^+$SL cells on day 6 after LCMV infection we co-transferred 10^3 MACS-purified (Miltenyi Biotec naïve CD8$^+$ T cell isolation kit, mouse) P14 WT and 3x10^3 MACS-purified P14 *Il1rl1*$^{-/-}$ cells into WT recipients in a set-up analogous to Figure 1J. These cell numbers were chosen for an equal recovery of P14 WT and P14 *Il1rl1*$^{-/-}$ cells on day 6 after infection. Mice were euthanized 5h after intraperitoneal administration of 1 mg 5-ethynyl-2'-deoxyuridine (EdU, baseclick, Germany). Splenocytes were then stained for surface markers followed by fixation for 15 min with 4% PFA. Cells were permeabilized using staining buffer supplemented with 0.05 % saponin (Sigma-Merck, Germany) for 20 min in the dark at RT. Detection of the incorporated EdU was performed according to the manufacturer's instructions (EdU-Imaging kit EdU-Click 488, baseclick).

In vitro activation of P14 WT cells and exposure to IL-33

Naive CD62L$^+$ CD44$^-$ CD8$^+$ T cells were sorted from spleens of P14 donor mice by flow cytometry and were cultured in the presence of a 4-fold excess of irradiated (3000 Gy) Tcrβδ$^{-/-}$ splenocytes in RPMI1640 $^+$ GlutaMax I (Thermo Scientific) culture medium supplemented with fetal calf serum (10% v/v, Thermo Scientific), penicillin (100 U/ml, Thermo Scientific), streptomycin (100 μg/ml, Thermo Scientific), gentamycin (10 μg/ml, Thermo Scientific), and β-mercaptoethanol (50 ng/ml, Sigma-Aldrich). For activation of P14 WT cells, cognate GP33 peptide (1 μg/ml, KAVYNFATM, Genscript), IL-12 (5 ng/ml, Miltenyi), IL-2 (5 ng/ml, Miltenyi) and anti-IL-4 (10 μg/ml, clone: 11B11, DRFZ) were added. T cells were split after 3 days of culture at a 1:3 or 1:5 ratio and supplemented with fresh medium containing IL-2 (5 ng/ml). After 5 days, P14 were harvested by histopaque (1083 g/ml, Sigma-Aldrich) density centrifugation and were replated for a second round of culture with fresh APCs in identical conditions as outlined above. At day 10 of culture, activated P14 cells were harvested, and live cells were seeded in culture medium containing IL-2 (5 ng/ml, Miltenyi) and IL-7 (5 ng/ml, Miltenyi) devoid of cognate peptide. After 3 days (day 13 of culture), IL-12 (5 ng/ml, Miltenyi) was added to induce IL-33 receptor expression and 14-16 h later (day 14 of culture), live P14 cells were harvested, replated in conditioned culture medium and stimulated with IL-33 (10 ng/ml, R&D Systems) for 2-6 h or left untreated. Proliferation of P14 cells was analyzed using the CellTrace Violet (CTV) Cell Proliferation Kit (Thermo Scientific). CTV labeling was performed according to manufacturer's instructions with the incubation time reduced to 10 min. For qRT-PCR analysis, 3-5x10^5 P14 cells per sample were lysed in RA-1 buffer (Macherey & Nagel) and immediately frozen in liquid nitrogen for storage at -80°C. Total RNA was extracted using the Nucleospin RNA XS Micro kit (Macherey & Nagel) according to manufacturer's instructions without addition of carrier RNA. Up to 1 μg of RNA was transcribed into cDNA utilizing Taqman Reverse Transcription Reagents (Applied Biosystems) according to the manufacturer's instructions and subjected to qPCR analysis using Taqman Fast Advanced Mastermix reagents (Applied Biosystems). Amplification was performed in a Quantstudio 7 device (Applied Biosystems) and *Tcf7* (Assay ID: Mm00493445_m1, Thermo Scientific) expression levels were quantified with the ΔΔCt-method by normalizing to expression levels of *Hprt* (Assay ID: Mm00446968_m1, Thermo Scientific).

Immunohistochemistry and image analysis

For immunofluorescence analysis on tissue sections, *Tcf7*^{gfp} P14 WT cells were MACS-purified (Miltenyi Biotec naïve CD8$^+$ T cell isolation kit, mouse) from the spleens of naïve donor mice and 10^6 cells were administered i.v. into the tail vein of recipients followed by LCMV infection. Animals were sacrificed at the indicated time points and spleens were fixed in 1% PFA in PBS, infiltrated with 30% sucrose and then embedded and frozen in OCT compound (Tissue-Tek, Sakura Finetek Europe). Cryostat sections (8μm) were collected on Superfrost Plus SLides (Fisher Scientific), air dried, preincubated with blocking solution (bovine serum albumine, normal mouse and donkey serum (Sigma) in 0.1% Triton/PBS followed by overnight labeling at 4°C with primary antibodies in

0.1% Triton/PBS. After washing with 0.1% Triton/PBS, the secondary detection reagents were applied for 2 hours at room temperature in 0.1% Triton/PBS. Finally, after additional washes the SLides were mounted in 1,4-Diazabicyclo[2.2.2]octan (DABCO). Sections were visualized following whole SLide image capture using a Hamamatsu NanoZoomer S60 and an 40x objective, utilizing a 8-bit color CMOS camera (Hamamatsu Photonics). Images were processed using NDP-view2 software (Hamamatsu Photonics) and Adobe Photoshop. Whole SLide images of serially cut sections were acquired with a resolution of 0.44 μm/px (Nanozoomer, Hamamatsu) and analyzed using Visiopharm (version 2021.09). The first of two sequential tissue cuts was stained for IL-33 and was used to define the IL-33-rich zone (''IL-33 zone''). This first section was overlaid and aligned with the second, sequential cut (TissueAlign module of Visiopharm) for transfer of the IL-33 zone (Figure 3H). The second cut was stained for IFN-α, CD45.1, B220 and GFP (*Tcf7*^{gfp}, Figures 3I–3K). CD45.1$^+$GFP$^+$ cells (for simplicity referred to as *Tcf7*$^{gfp+}$ or GFP$^+$ in Figure 3 and its accompanying figure legend) in the IL-33 zone were detected and their distance to the closest IFN-α expressing cell was calculated to determine the proportion of *Tcf7*^{gfp} within a 20μm perimeter of an IFN-α-producing cell. IL-33- and IFN-α-producing cells (Figure S3L) were stained and detected together on one tissue cut.

QUANTIFICATION AND STATISTICAL ANALYSIS

For statistical analysis GraphPad Prism software (Version 9.0, Graph Pad Software) was used. Differences between two groups were assessed by using an unpaired two-tailed Student's t-test. Differences between two cell populations within in the same host (co-transfer set-up) were assessed by using a paired two-tailed Student's t-test. For multiple pair-wise comparisons in one experiment we performed Student's t-tests with Bonferroni correction. For single-parameter comparisons between more than two groups one-way ANOVA with Tukey's or Sidak's post-test was performed. For multiple comparisons of multiple parameters between two or more groups and for time kinetics two-way ANOVA with either Tukey's or Sidak's post-test was performed. Ns: not statistically significant; *: $p<0.05$; **: $p<0.01$. Absolute numbers were log-converted to obtain a near-normal distribution for statistical analysis.